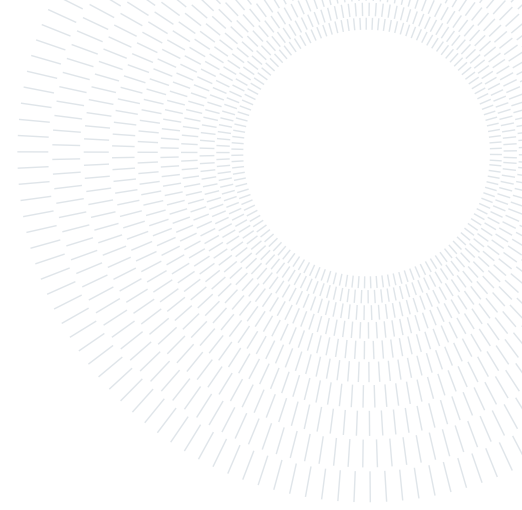




POLITECNICO
MILANO 1863

**SCUOLA DI INGEGNERIA INDUSTRIALE
E DELL'INFORMAZIONE**



Clustering Neuron Population Spike Data and Assessing Cortical Area Connectivity

TESI DI LAUREA MAGISTRALE IN

BIOMEDICAL ENGINEERING - INGEGNERIA BIOMEDICA

The dissertation was conducted at the Laboratory of Sensory Processing at EPFL

Reza Asri, 943119

Advisors:

Prof. Alessandra Pedrocchi
Dr. Sylvain Crochet

Co-advisors:

Prof. Carl Petersen
Dr. Vahid Esmaeili
Anastasiia Orishchuk
Alireza Modirshanechi

Academic year:

2022-2023

Abstract: The interpretation of incoming sensory information from the outside world to guide adaptive behavior is a crucial function of the brain. A fundamental question in neuroscience is how and where sensory information is translated into motor commands in a context- and learning-dependent manner. Studies have demonstrated a gradual transformation of sensory signals into decision/motor signals from sensory to frontal areas: primary sensory areas encode primarily the physical features of the stimulus, whereas the response of frontal areas (such as the prefrontal cortex) covaried with both the decision and the physical features of the stimulus. Thus, it has been argued that flexible sensorimotor decisions result from the integration of sensory and task information in the prefrontal cortex. The medial prefrontal cortex (mPFC) is assumed to play a fundamental role in context-dependent behaviors. In this study, a clustering algorithm was developed on top of neuronal firing rate (spikes) data to group neurons with similar behavior in order to better investigate their function in sensorimotor integration. It has been discovered that there are clusters of wS1 and tjM1 neurons that primarily contribute to sensory and motor coding, respectively. In contrast, other sensory or motor-related neurons are widespread in other areas. Clusters dominated by mPFC neurons display complex behaviors that may reflect the mPFC's potential function in improving learning through error (teaching) signals. In a separate study, it is investigated how learning contributes to brain plasticity by measuring changes in connection between sensory and motor regions during goal-directed learning of a specific task. The findings demonstrated that learning changes the connections between neurons from wS1 to wM1 and from wS2 to wM1 differently.

Key-words: Sensory-Motor Integration, Neuronal Clustering, Neural Connectivity

1. Introduction

Neurons (nerve cells) are the essential units of the brain and nervous system, responsible for processing sensory information from the outside world, delivering motor commands, and altering and relaying electrical signals at every step in between. A key function of the nervous system is the interpretation and control of behavior in response to incoming sensory input from the outside world. Every instant, the brain simultaneously receives a vast amount of sensory information from various sensory organs. Even in animals with smaller and less complex neural systems, such as the medicinal leech, basic tactile stimulation can trigger context-dependent behaviors such as local bending, crawling, or swimming [18]. Multiple factors influence how the brain chooses the most appropriate action to do in response to a given stimulus. For example, if you are traveling through the forest and you tread on a dead branch, causing it to snap and produce a cracking sound, and then you feel something on your foot, you may have stepped on an object. You conclude that the object you walked on maybe a splinter from a fallen branch, so you continue walking. In contrast, if you hear the sound of a rattlesnake and then feel something on your feet, you may respond quickly since the object could be a snake. Similar touch sensations should be processed and interpreted context- and experience-dependently in this prospective scenario. The location and mechanism of these sensorimotor transformation in the brain is a fundamental subject in neuroscience. This question has been primarily studied for decades utilizing extracellular recordings in various cortical regions of monkeys executing complex sensory detection or discrimination tasks. Combining psychophysical and neurophysiological experiments in monkeys performing a tactile detection task, De Lafuente and Romo [6] discovered that the activity evoked by the sensory stimulus is propagated from early somatosensory cortices to many areas, including association and motor areas. To evaluate the role of distinct recording areas in the processing of sensory stimuli, the researchers measured how the stimulus amplitude influenced the normalized neuronal firing rate using linear regression analysis. Higher-order areas do not encode stimulus amplitude with the same precision as the early somatosensory cortex (Figure 1). Similarly, neuronal activity in primary somatosensory area (S1) was not predictive of subject outcomes, whereas neuronal activity in higher-order cortical regions was highly linked with behavioral outcomes [6].

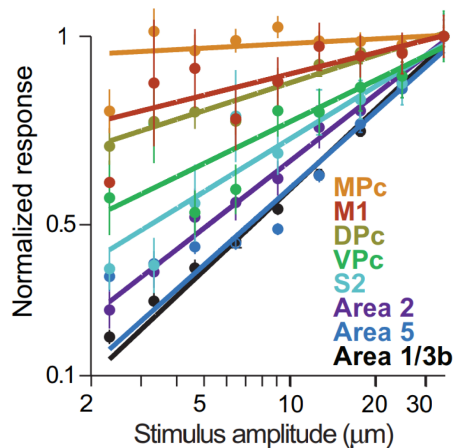


Figure 1: Encoding of stimulus amplitude across cortical areas during the detection task. Mean normalized firing rates as a function of stimulus amplitude. Colored lines are best linear fits to the firing rate as a function of the logarithm of the amplitude. MPC: medial premotor cortex, M1: primary motor area, DPc: dorsal premotor cortex, VPc: ventral premotor cortex, S2: secondary somatosensory cortex, and Area 2, 5, 1, 3b: corresponding Brodmann areas. Adapted from [6].

Various investigations concluded that sensory, motor, and decision-related signals are represented in multiple brain regions, including the dorsolateral prefrontal cortex, but no one region can be identified as the place where sensory information is transformed into motor commands [37]. Sensory input is frequently noisy and unpredictable, and the perception of certain stimuli, such as visual random dot motion [39], needs spatial and temporal integration. With precisely timed spiking activity, neurons in early sensory areas encode the stimuli’s physical properties. As a result, S1 is not the best area to combine spatio-temporal data. Therefore, higher cortical circuits must integrate over time to reflect specific whisker stimulation sequences [13].

To investigate the neuronal circuits responsible for goal-directed sensorimotor transformation with single-cell resolution and to address the causal role of well-defined neuronal populations, many researchers are currently employing mice as an animal model and implementing well-controlled behavioral tasks with the aid of advanced technology. Mice are crepuscular animals that rely mostly on tactile information to navigate in the dark [49]. Whiskers are active sensors that can move back and forth to assess the animal’s immediate physical environment. Mice and rats use their whiskers to sense minute vibrations, pinpoint objects, and execute extremely fine texture and aperture discrimination [7, 34]. The whiskers are topologically arranged in rows and arcs, and this arrangement is maintained along the neural pathway that conveys sensory information from the periphery to the whisker primary somatosensory cortex (wS1), also called the barrel cortex (Figure 2A). The physical deflection of the whiskers stimulates the follicle’s mechanoreceptors [4]. This tactile information is subsequently relayed by the brainstem and thalamus to wS1 (Figure 2B) [7, 34].

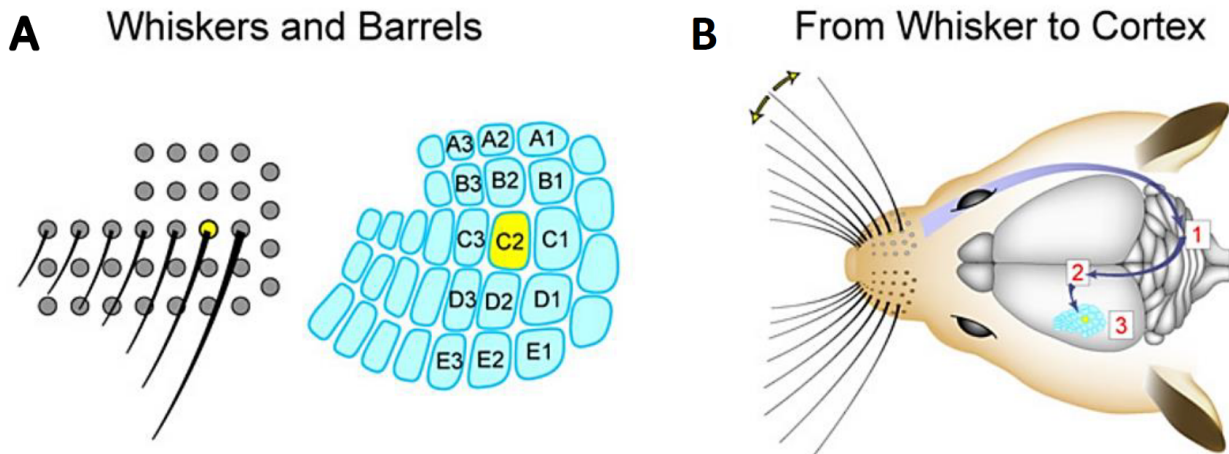


Figure 2: Synaptic pathways for processing whisker-related sensory information in the mouse barrel cortex. (A) The layout of whisker follicles (left) on the snout of the mouse. Anatomical structures are termed “barrels” in layer 4 of the primary somatosensory neocortex (right), which are laid out in a nearly identical pattern to the whiskers. (B) (1) The deflection of a whisker evokes action potentials in sensory neurons of the trigeminal ganglion, which release glutamate at a first synapse in the brainstem. (2) The brainstem neurons send sensory information to the thalamus, (3) where a second glutamatergic synapse excites thalamocortical neurons projecting to the primary somatosensory barrel cortex. Adapted from [34].

A single whisker deflection elicits reliable sensory responses in wS1. The response of neurons in wS1 varies according to the stimulus’s physical characteristics. The whisker deflection’s amplitude and frequency influence the activity of wS1 neurons [46]. Neuronal activity in wS1 is essential for the execution of various whisker-based perceptual goal-directed tasks in mice, such as object localization [29], texture discrimination [50], and detection of a single whisker deflection or vibration [4, 19, 20, 27, 34, 38]. In head-fixed mice trained to lick a waterspout in response to a brief single-whisker deflection, inhibiting the sensory-evoked response in wS1 significantly reduces the chance of licking, showing the critical role of barrel cortex neuronal activity for the detection of the whisker stimulus [38]. Therefore, wS1 is a well-defined early stage for whisker sensory stimulus conversion into goal-directed motor action (licking). In contrast to sensory regions, the correlation between neuronal activity in motor regions and motor action is the strongest. Whisker motions are associated with the neuronal activity of the whisker motor cortex (wM1) [17, 45]. Single-cell stimulation within the motor cortex can elicit minute but considerable whisker movements [3]. Optogenetic stimulation of the whisker motor cortex induces whisker protraction, whereas Opto-inhibition dramatically reduces whisker movement [8, 45]. Although wM1 receives direct inputs from wS1, it does not control licking and is not required for the whisker-based detection task to be performed [20]. In a recent study, as identified the tongue/jaw primary motor cortex, an additional part of the motor cortex that controls tongue and jaw motions (tjM1). tjM1 neurons encode licking movements with strong selectivity for licking direction (left or right); unilateral activation of tjM1 drives licking in the contralateral direction, while unilateral inhibition inhibits contralateral licking [26]. Thus, tjM1 is likely the endpoint of the sensorimotor transformation in which a short whisker deflection is transformed into goal-directed licking to receive a reward. tjM1 receives direct sensory inputs from the primary sensory cortex of the tongue and jaw, but it does not receive input from wS1. The transformation of whisker sensory input into a motor command must therefore involve other cortical and subcortical regions. How and where does this sensorimotor transformation occur in the brain? Even during the execution of a basic whisker-based detection task in mice, sensory-related neuronal activity rapidly spreads across various cortical areas, with short latencies (less than 50 ms) reaching the medial prefrontal cortex and dorsal hippocampus [20]. Important for the organization of goal-directed behavior, the prefrontal cortex (PFC) encodes different types of information from all phases of the perception–action cycle. Neurons in the prefrontal cortex (PFC) of non-human primates have been found to respond to stimuli from several sensory modalities. For instance, PFC cells respond selectively to both tones and colors based on the task rule [14], indicating that PFC neurons represent cross-modal associations with behavioral meaning. The activity of PFC neurons has also been found to covariate with the choice of the primates as well as the sensory information. [24] and [40] established that during a sensorimotor decision, PFC contains both sensory and choice information. By modeling the population dynamics of PFC neurons, they hypothesized that the integration of sensory and task information leads to the development of flexible sensorimotor decisions in the prefrontal cortex [24, 40]. Although mPFC is believed to control behavior by integrating different rules in complex tasks, it also appears important for the execution of simple sensory detection or discriminating tasks in mice [20, 31, 35]. Similar to the literature on primates, mouse mPFC neurons exhibit a wide range of task-related activity: they respond to sensory signals, motor output, and action outcomes [35]. The major benefit of utilizing mice as a model system is their genetic tractability, which allows for the monitoring of the activity of specific cell types and projection neurons. Different cortical layers’ neurons receive various inputs and project to distinct target regions, and their local circuit interconnections play essential roles in information processing. This strategy is crucial in the mPFC, where neurons frequently exhibit multiplexed encoding features. During a simple Go/NoGo task, [35] investigated the neuronal activity of genetically different cell types in the mPFC. In this experiment, a light flash signaled the beginning of each trial, which was then followed by either a target-signal (17 kHz acoustic stimulus) or a nontarget-signal (9 kHz acoustic stimulus). The animal’s lick response was rewarded if the target signal was presented and penalized if the nontarget signal was presented following the stimulus presentation. In this experiment, pyramidal neurons constituted a heterogeneous population whose functional responses differed between layers. Following a relevant sensory input, these neurons displayed both excitatory and inhibitory response. Nevertheless, inhibitory interneurons signaled distinct task-related events. The activity of the majority of somatostatin (SST) positive neurons was associated with licking behav-

ior, whereas the activity of vasoactive intestinal peptide (VIP) positive neurons was significantly modified by the action outcome. Parvalbumin (PV) positive neurons were the least selective and exhibited the most robust responses to sensory stimuli [35]. The experience greatly influences the neuronal activity of pyramidal cells in the medial prefrontal cortex. During learning, mPFC neurons respond primarily to behaviorally relevant sensory stimuli and do not respond to unrewarded stimuli [20, 31, 35]. The presence of a sensory-evoked response in the mPFC after learning may indicate that the mPFC may play many functions in the sensorimotor transformation.

To determine which neurons are involved in a particular aspect of sensorimotor task, scientists usually rely on simple methods. Past methods relied on inspecting huge populations of neurons and classifying them into subpopulations based on the investigator’s knowledge and experience [43]. In circumstances where neuron populations are small, it is reasonable to closely study these neuronal recordings and their firing rates to prevent data omissions. Clustering is an unsupervised learning technique that aims to identify the underlying data structure by grouping data points based on similarity. The advancements in neuroscience have produced huge and complicated data sets, making clustering vital for data comprehension and visualization. Major studies like [9, 15, 22, 30, 48] utilised unsupervised clustering on neural data to create groups of neurons with the same behavior in order to explore the neural behavior of a large recorded population of neurons and their hypothesized roles more precisely. By defining the properties of neurons within a specific group, the researcher can then determine functional classes of neurons depending on their relationship to the task. Convolutional neural network (CNN) is among the most used algorithms for the clustering of the primary visual cortex neurons as it imitates the behavior of the groups of neurons in primary visual cortex (V1) in feature extraction of the visual field, however, for sensorimotor areas the most used method is gaussian mixture model (GMM). The concept is based on collecting significant features from the firing rate and clustering them using an expectation-maximization Gaussian mixture algorithm (EM-GMM) [30]. The approach can automatically detect and cluster similar firing rate profiles based on specific signal characteristics. A Gaussian mixture model is a probabilistic model in which it is assumed that all data points are generated from a mixture of a finite number of Gaussian distributions with unknown parameters. The gaussian mixture object implements the expectation-maximization (EM) approach for fitting mixture-of-Gaussian models. The Expectation Maximization method is iterative and it begins with an initial parameter guess. The parameter values are used to calculate the model’s likelihood which corresponds to Expectation step. The parameter values are subsequently recalculated to maximize the probability. Therefore, expectation maximization provides an iterative solution to the maximum likelihood estimation of the correspondence of a neuron to a specific cluster with latent variables. In addition, Bayesian Information Criterion to evaluate the number of clusters in the data could be calculated. Mixture models are a generalization of k-means clustering that incorporates the covariance structure of the data and the centers of the latent gaussians. Consequently, GMM outperforms k-means clustering in modeling complex points distributions in feature space which merely partitions data in K clusters based on distance metrics. The benefit of using the EM algorithm for maximizing the expectation of a data point being within a single cluster given our parameters and data is that it is always guaranteed an increase in likelihood after each iteration, whereas many numerical solutions frequently get stuck in suboptimal localized wells. In addition, the E-step and M-step are far simpler to calculate than complex reparameterization measures, which are frequently counterintuitive and may not always guarantee the ideal answer.

To investigate the role of learning in the modification of synaptic connections and assess brain plasticity, functional connectivity study of neuron-to-neuron or network-to-network was utilised. Neural plasticity, also referred to as neuroplasticity or brain plasticity, is the capacity of the nervous system to change its activity in response to intrinsic or extrinsic stimuli by reorganizing its structure, functions, or connections. Findings show that the brain’s connection increases quickly in time in both humans and other animals over Developments. This mechanism has been explored most thoroughly in the brain’s cortex, which is essentially our gray matter. Researchers have demonstrated that the number of synapses per unit area or unit volume of cortical tissue, along with the number of synapses per neuron, fluctuate during the span of our lifetimes. The number of synapses

per unit of cortical tissue is referred as to the brain’s synaptic density. Our brain’s synapse density evolves in a fascinating, regular way over the course of our lives. Through their synaptic connections, brain cells construct the neural circuits that support our sensory, motor, and cognitive abilities and eventually govern our entire behavior. Neurons differ in a range of shapes and sizes, but all possess a cell body including a nucleus. The majority of neurons have extensions from the cell body. Axons, the lengthy branches of cells (which are typically encased in a myelin sheath), transport nerve impulses from the cell body to neighboring neurons. Dendrites, which are the shorter branches, receive impulses from pre-synaptic neurons and send them to the cell body. Typically, nerve cells are not in physical contact with one another. There are small gaps between the axons and dendrites of neighboring neurons. Through these small spaces called synapses, communication between neurons occurs. Chemical neurotransmitters pass from the pre-synaptic end of the axon to the post-synaptic membrane of the next dendrite across the gaps. The electrical activity of the postsynaptic cell is then either excited or inhibited by these chemical messengers. Cortical neurons can have various direct (mono-synaptic) and indirect synaptic functional interactions with neurons both within and outside their local processing units through intermediate neural networks. Correlation exists between the firing activity of cortical neurons and are thought to be a key in processing of many neural systems. For instance, neurons share trial-to-trial variations in response strength, and spikes frequently occur synchronously [44]. To determine the function of these forms of correlation in cortical processing, it is essential to comprehend the qualities and mechanisms that generate them. Therefore, it was decided to investigate how neural connectivity changes across learning and training of the mice. The functional connectivity by correlation analysis was evaluated since typically, cortical neurons are contained within a processing unit, such as a column or a local microcircuit. To be more precise and to overcome the flaws of correlation analysis in spike data, researchers used spike time tiling coefficient (STTC) method [5] as it is difficult to quantify correlations for two reasons. First, correlated neurons fire at similar times but not precisely synchronously; therefore, correlation must be described in terms of a timescale within which spikes are considered correlated. Second, spiking is sparse regarding the recording’s sampling frequency and spike duration. This implies that conventional approaches to correlation (such as Pearson’s correlation coefficient) are inappropriate, as periods of quiescence should not be counted as correlated and correlations should compare spike trains over short time frames, not just instantaneously. The spike time tiling coefficient uses the proportion of the recording that falls within Δt of spikes from neuron A to evaluate if the proportion of spikes in neuron B that share this property is indicative of the correlation. Due to the fact that tile overlaps are not counted several times, this is dependent on both firing patterns and rates. In the correlation index, only the firing rates are used to figure out what is expected by chance, whereas firing patterns are crucial. Cross-correlogram method was also implemented to assess mono-synaptic directional connectivity [40] as neurons in the cerebral cortex create thousands of synapses with other cortical neurons in nearby and distant brain regions and have descending and recurrent connections with subcortical systems [28]. For the interpretation of the cross-correlogram, if the peak lies temporally after the center bin in the cross-correlogram between neuron i and j , neuron i is pre-synaptic with regard to neuron j , and vice versa. It has been found out that wS1 and wS2 neuronal activity can only contribute to task performance via communicating with other brain regions. In addition to different subcortical projections [42, 47], the innervation of frontal cortical regions may play a crucial role in linking sensation and movement [11, 12]. It has been demonstrated that wS1 neurons innervate wM1 [2, 25], but much less is known about the long-range output of wS2 which is going to be discussed in this study.

1.1. Aim of the work

(1) To analyze and create a method for clustering large populations of neurons based on their firing rate activity. Neurons belonging to the same cluster share the same firing pattern, allowing them to encode together particular sensorimotor transformation characteristics. (2) To evaluate the functional and causal connections between some areas simultaneously recorded to investigate learning-related changes in brain plasticity.

2. Methods

This master's thesis is done as a data analyst internship at EPFL university and data used in clustering and connectivity projects are respectively titled as "Psychometric detection task" and "Delayed response detection task" gathered by neuroscientists at EPFL's laboratory of sensory processing.

2.1. Surgical procedure

The surgical procedures of psychometric detection task and delayed response detection task are remarkably similar; therefore, to minimize duplication, only surgical procedure of psychometric detection task is described here.

2.1.1 Implantation of metal headpost

Mice were thoroughly anesthetized with isoflurane (3 percent with O₂) and maintained under anesthesia by an intraperitoneal injection of ketamine and xylazine (ketamine: 125 mg/kg, xylazine: 10 mg/kg). Analgesic carprofen was given intraperitoneally (100 ml at 0.5 mg/ml) before to the beginning of surgery. Using a heating pad, the body temperature was maintained at 37°C during the procedure. To prevent the eyes from drying out, an ocular ointment (VITA-POS, Pharma Medica AG, Switzerland) was rubbed over them. Before surgical intervention, a mixture of lidocaine and bupivacaine was injected beneath the scalp as a local anesthetic. For skin disinfection, a povidone-iodine solution (Betadine, Mundipharma Medical Company, Bermuda) was utilized. Using surgical scissors, a portion of the scalp was cut to expose the skull. Using cotton swabs and a scalpel blade, the periosteal tissue was removed. After disinfecting the cranium with Betadine and rinsing it with Ringer solution, cotton buds were used to dry it thoroughly. A thin coating of superglue (Loctite superglue 401, Henkel, Germany) was then applied over the dorsal portion of the skull, and a custom-made head fixation implant was attached to the right hemisphere without a tilt and in parallel with the midline. On the left hemisphere, a second uniformly distributed coat of glue was placed. After the glue had dried, the head implant was additionally fixed with self-curing denture acrylic (Paladur, Kulzer, Germany; Ortho-Jet, LANG, United States). For electrophysiological recordings, a chamber was created by constructing a denture acrylic wall along the edge of the left hemisphere bone. This entire, clear skull preparation was used for imaging research involving intrinsic optical signal (IOS). After surgery, mice were returned to their home cages and given ibuprofen (Algifor Dolo Junior, VERFORA SA, Switzerland) in their drinking water for three days.

2.1.2 Skull preparation and craniotomies

For intrinsic optical imaging, an intact, transparent skull was utilized. Using a dental drill and isoflurane anesthesia, up to three minor craniotomies were done over the regions of interest for electrophysiological recordings. The craniotomies were protected with a silicon elastomer (Kwik-Cast, World Precision Instruments, Sarasota, Florida, United States). The hotspots of activity from IOS imaging were used to select regions of interest [21]. Under isoflurane anesthesia, IOS was done to map the C2-whisker representation in primary whisker somatosensory cortex (wS1). Utilizing a magnetic actuator, the right C2 whisker was vibrated. Increased red light (625 nm) absorption in response to sensory stimulation indicated the location of the associated sensory cortex. For the remaining regions, stereotaxic coordinates relative to the bregma were employed: primary tongue/jaw motor cortice (tjM1: AP 2.0 mm; LM 2.0 mm), medial prefrontal cortex (mPFC: AP 2.0 mm; LM 0.5 mm).

2.2. Behavioral paradigm of psychometric task and extra-cellular recording

Mice were trained head-restrained to perform a whisker dependent tactile detection task during which a brief passive C2 whisker stimulation is present and mice respond by licking a spout in order to obtain a reward

(Figure 3A). The whisker stimulation was achieved by attaching an iron particle to the C2 whisker (1 mm from the pad) at the beginning of each training session. A magnetic coil placed directly below the mouse's head produced a 1 ms magnetic pulse, which was subsequently used to induce a small and rapid whisker movement. This stimulation of whisker caused a vertical passive deflection. The magnetic pulse was produced by loading the coil with a 1 ms-long biphasic voltage pulse using a high-power amplifier. Over sessions, mice learned to lick in response to the whisker stimulus within the one second response window after stimulus onset. Mice were also required not to lick for a variable 2.5-3.5 s 'No Lick' window in order to initiate a new trial (Figure 3B). Mice were presented with four different whisker stimulation amplitudes from very low (1 degree) to salient (3.3 degree) randomly interleaved during the behavioral session. Trials when the mouse licked the reward spout within the 1 second response window after whisker stimulation, were considered as "hit trials", and rewarded with the sweet water; if the animal did not lick within one second of response window after whisker stimulation no reward was delivered, and these trials were considered as "miss trials"; trials when no whisker stimulation were delivered (catch trials), but the mouse licked the reward spout were considered as "false alarm trials"; if no licking occurred during catch trials, they were considered as "correct rejection". Once the performance of the animal reached a stable and satisfactory level (more than 70 percent of hit rate and less than 30 percent of false alarm for the strongest amplitude), an acute extracellular recording session was performed using silicon probes as mice performed the psychophysical task. Two areas out of three areas were recorded simultaneously (Figure 4B). Neuronexus silicon probes (NeuroNexus Inc.) were used with 32 recording channels spanning 775 μm in length (Figure 4A). In each session, two probes were implanted into two distinct brain sites. For post hoc retrieval of the recording location, probes were coated with DiI.

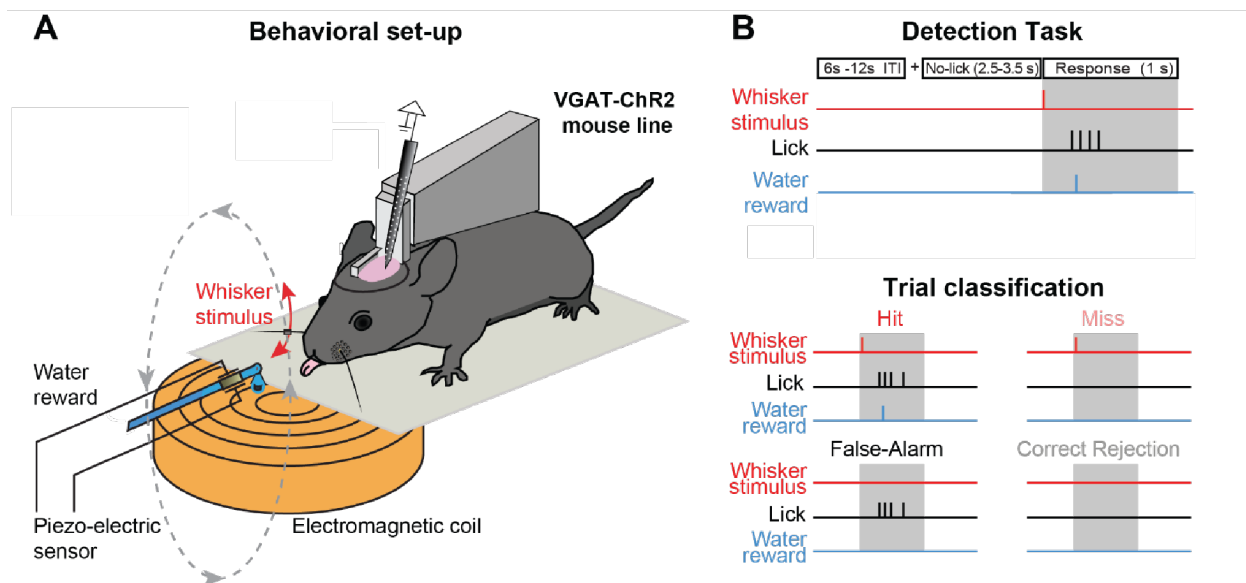


Figure 3: Experimental setup and recording methodology. (A) The experimental setup for the whisker-based detection task. Mice were head-restrained in front of a water spout and above an electromagnetic coil. A metal particle was attached to the C2 whisker, which was deflected by a 1-ms magnetic pulse. (B) Task structure. Animals were trained to respond to the whisker stimulation by licking the reward spout within the 1 s of the response window and to suppress licking for a random interval of 2.5-3.5s during no lick period. Trials were separated by a 5-10 s inter-trial interval. Stimulus trials and non-stimulus trials (Catch trials) were randomly interleaved. In total four trial types were considered: Hit, Miss, False-alarm, Correct rejection.

Extracellular recording with silicon probe

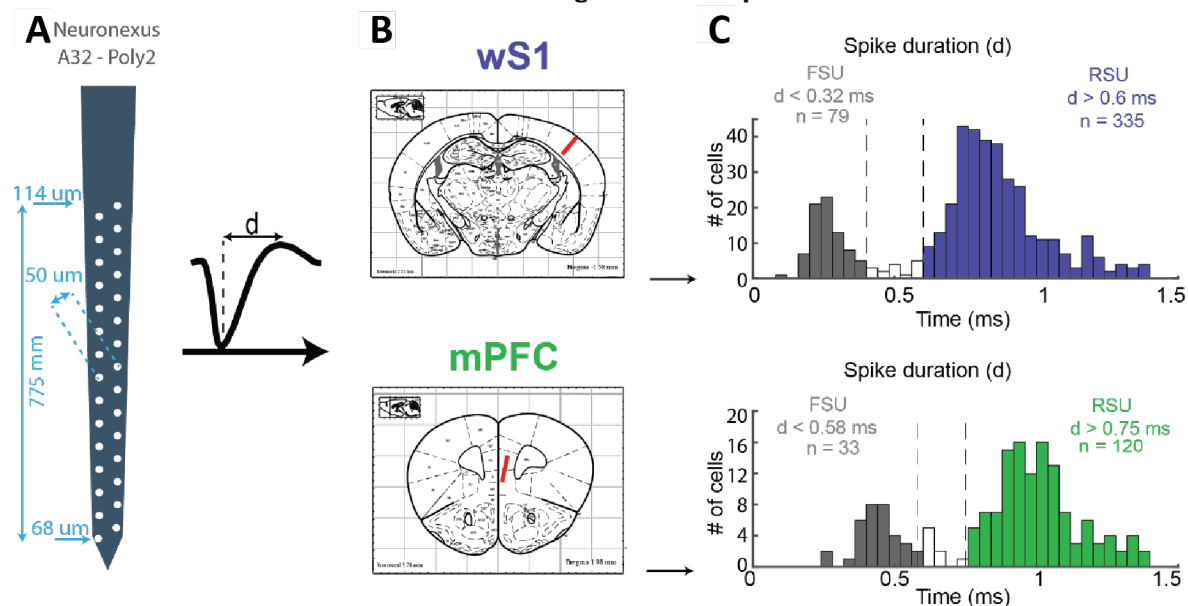


Figure 4: (A) Schematic representation of the probe dimensions. (B) Schematic representation of the targeted recorded positions for wS1 and mPFC. (C) Histogram of spike durations for wS1 (upper plot) and mPFC (lower plot). Spike duration was calculated as a time from the negative peak of the mean waveform of the spike to its positive peak.

2.3. Behavioral paradigm of delayed response task and extra-cellular recording

In another task, a go/no-go learning paradigm was designed where head-restrained mice learned to lick in response to a whisker stimulus after a 1-s delay period (Figure 5A- 5C). Each trial included a visual cue (200 milliseconds, green LED) and an auditory cue (200 ms, 10 kHz tone of 9 dB added on top of the continuous background white noise of 80 dB). The stimuli were separated by a delay interval that was gradually increased to 2 seconds during the course of the pretraining days. A total of 55 mice were trained in the delayed whisker detection task including 9 RCaMP, 24 wild-type or negative, 6 *Emx1-ChR2*, 9 *VGAT-ChR2* and 7 *tdTomato* mice. During the behavioral studies, all whiskers were trimmed with the exception of the C2 whiskers on both sides, and the mice were given 1 mL of water per day. Mice were trained daily with one training session every day, and their weight and overall health status were carefully tracked using a score sheet. Expert and Novice mouse groups underwent a pretraining phase consisting of trials with visual and auditory signals (without whisker stimulus) (Figure 5C). Mice were rewarded for licking a spout placed on their right side within one second after the onset of the auditory cue. Trials were separated by 6 to 8 seconds and began after a time of 2 to 3 seconds during which mice did not lick the spout. Licking before the response period (Early lick) aborted the trial and introduced a 3-5 s timeout. Mice learned to lick the spout by detecting the auditory cue and suppressing early licking after 3-6 days of pretraining. The electrophysiological recordings from the Novice group of mice was performed when mice finished the pretraining phase and were introduced to the whisker delay task (Figure 5C). In half of the trials, a whisker stimulus (10 ms cosine 100 Hz pulse through a glass tube attached to a piezoelectric actuator) was applied to the right C2 whisker 1 s following the beginning of the visual cue. Importantly, the reward was only accessible in trials with the whisker stimulus (Go trials), and mice who licked in trials without the whisker stimulus (No-Go trials) were punished with a time-out and an auditory buzz tone (Figure 5B). Thus, mice were trained to change their licking/non-licking behavior in response to the whisker stimuli. Since the whisker stimulus was weak, Novice mice continued to lick in the majority of Go and No-Go trials regardless of the whisker stimulus and exhibited no whisker learning (Figures 5D). The Expert mice entered a 2-29 day Whisker-training phase during which a stronger whisker stimulus (larger amplitude and/or pulse train) and shorter delays (for some mice) were introduced. As the mice learnt to lick properly, the

whisker stimulus amplitude was gradually decreased and the latency was increased to 1 s, eventually achieving the same circumstances as novice mice. As measured by the piezoelectric lick sensor, expert mice decreased licking in No-Go trials but increased their premature early licks after the whisker stimulus (Figure 5D).

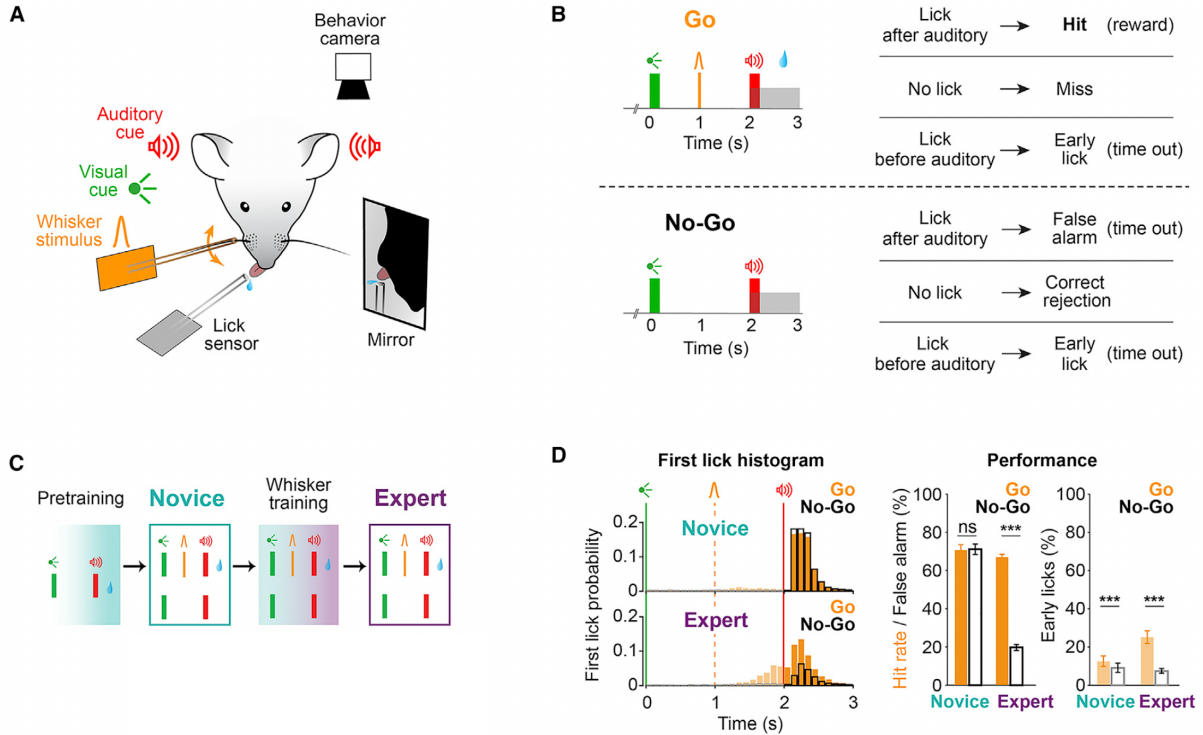


Figure 5: (A and B) Delayed whisker detection task. (A) Behavioral setup. Sensory stimuli were delivered to head-restrained mice, and licking and orofacial movements were monitored using a piezoelectric lick sensor and a behavior camera. (B) Task structure and trial outcomes in go and no-go trials. (C) Learning paradigm. All mice went through visual-auditory pretraining, where all licks after the auditory cue were rewarded. Expert mice went through whisker training, where final task structure was used as in (B). Neural data were obtained using the final task design in novice mice before and after whisker training, respectively. The same mice were imaged during novice and expert stages, while different mice were used for electrophysiological recordings. (D) Task performance. Left: first-lick time histogram was similar in go versus no-go trials in novice mice but differed in expert mice. Early licks (licks between visual cue and auditory cue) are shown with light colors. Middle: novice mice licked equally in go and no-go trials, whereas expert mice licked preferentially in go trials (quantified as mean \pm SEM across all completed trials; novice, $n = 15$ mice; expert, $n = 25$ mice). Right: both groups of mice made more early licks in go compared to no-go trials. *** indicates $p < 0.001$ according to Wilcoxon signed-rank test.

2.4. Experimental design

Randomization and blinding were absent from these studies. Prior to doing the study, they did not estimate sample size. Nevertheless, this study’s sample size is equivalent to that of previous researches [22, 36].

2.5. Localization of electrode

At the end of the experiment, the mice were perfused with phosphate-buffered saline (PBS) followed by 4 percent paraformaldehyde in PBS (PFA, Electron Microscopy Science, USA). The brain was post-fixed at room temperature overnight. Either two-photon tomography [26] or standard histological examination was utilized

to identify the DiI track of silicon probes.

2.6. Pre-analysis of electrophysiological data

Using a digital headstage, the neural input was filtered between 0.3 Hz and 7.5 kHz and amplified. The headstage used a sampling frequency of 30 kHz to digitize the data. The signal was transmitted to our data gathering system and stored on the host PC’s internal HDD for offline processing. Spike sorting was performed offline using Kilosort algorithm [32]. Single units were isolated and separated into fast-spiking units (FSU) or regular spiking units (RSU) based on spike width (Figure 4C).

2.7. Clustering analysis of psychometric neuronal (Spikes) data

The analysis included RSUs from Expert mice ($n = 1598$ out of 2001 total RSUs and FSUs) for clustering the neural response patterns. 5 kinds of trials are included in the analysis; hit trials aligned both to whisker stimulus onset and to jaw opening onset; miss trials aligned to whisker stimulus onset; spontaneous licks happening in inter-trial intervals and aligned to the lick signal from piezo sensor on water spout; spontaneous whisking trials that are aligned to the onset of whisking. For each neuron and trial type, time-varying PSTHs (100 ms bin size) were generated during a 2.5-s window beginning 1 s before the alignment and ending 1.5 s afterward (25 bins for each kind of trial). PSTHs from various trial types were baseline subtracted, normalized to the range of values across all bins (of all five trial types), and then concatenated, yielding an activity matrix $X \in \mathbb{R}^{1598 \times 125}$ whose row i corresponds to the concatenated normalized firing rate of the neuron i across various trial types and columns correspond to time bins (Figure 7). Grand average PSTHs for each recorded area is separately calculated (Figure 8). Other techniques, such as z-scoring, produced comparable clustering results.

A general overview of steps taken for clustering is shown in Figure 6. To decrease the existing redundancy between firing rate time bins and speed up the computation, principal component analysis (PCA) was applied to linearly projected firing rate vectors onto a low-dimensional space removing correlated features before clustering. PCA was performed on the centered version of X (i.e., $x_i - \bar{x}_i$) and identified nine significant components (Figure 9) (permutation test with Bonferroni correction to control the family-wise error rate to 0.05) [23].

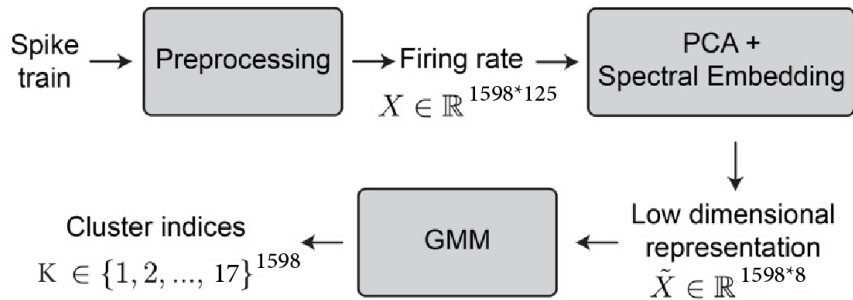


Figure 6: Block diagram indicating the different steps for unsupervised neuronal clustering. Dimensionality reduction and spectral embedding were applied on concatenated trialtype averaged PSTHs of neurons and the results were clustered by fitting a Gaussian mixture model (GMM).

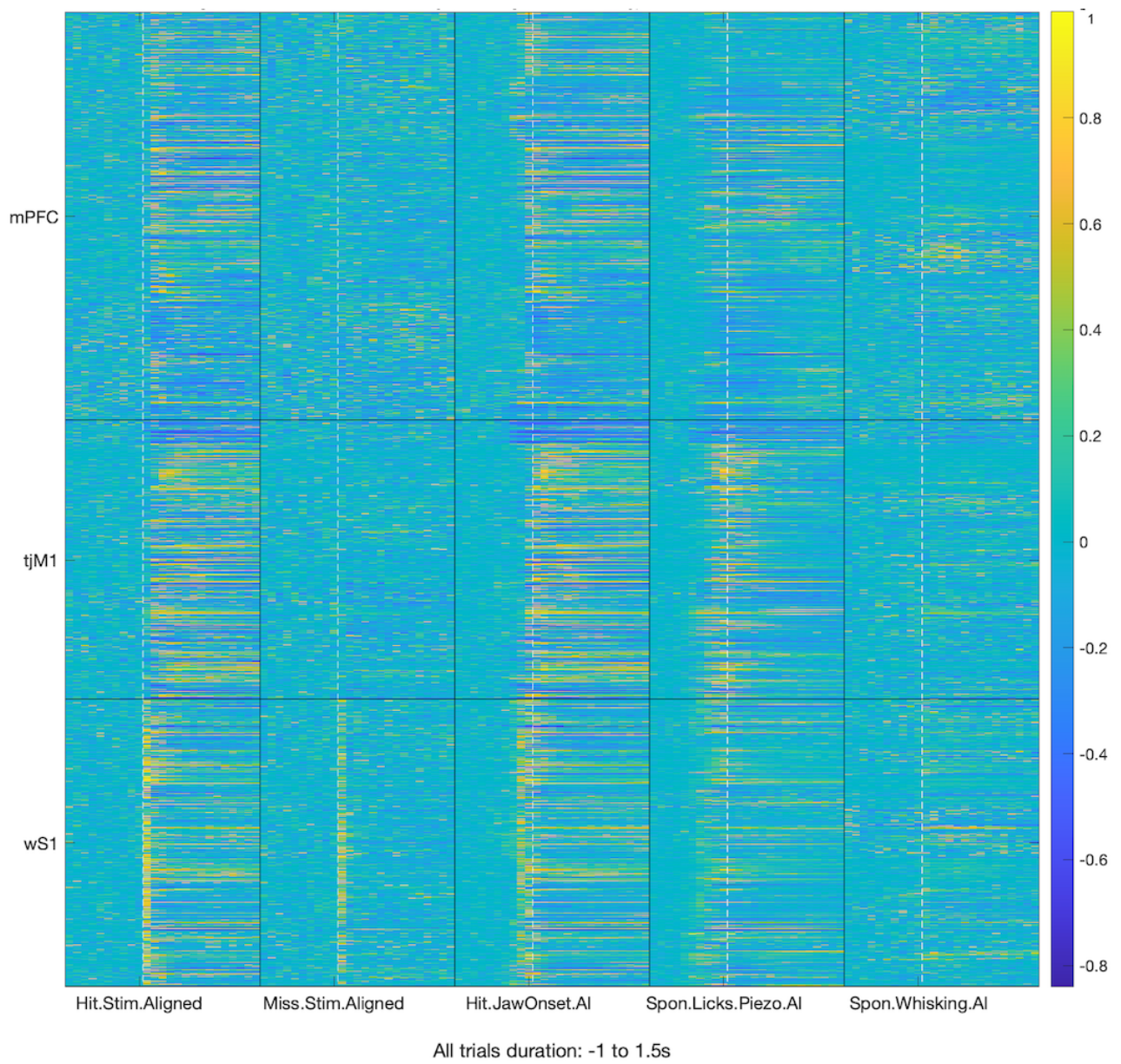


Figure 7: PSTH of matrix X. Color bar represents normalized firing rate.

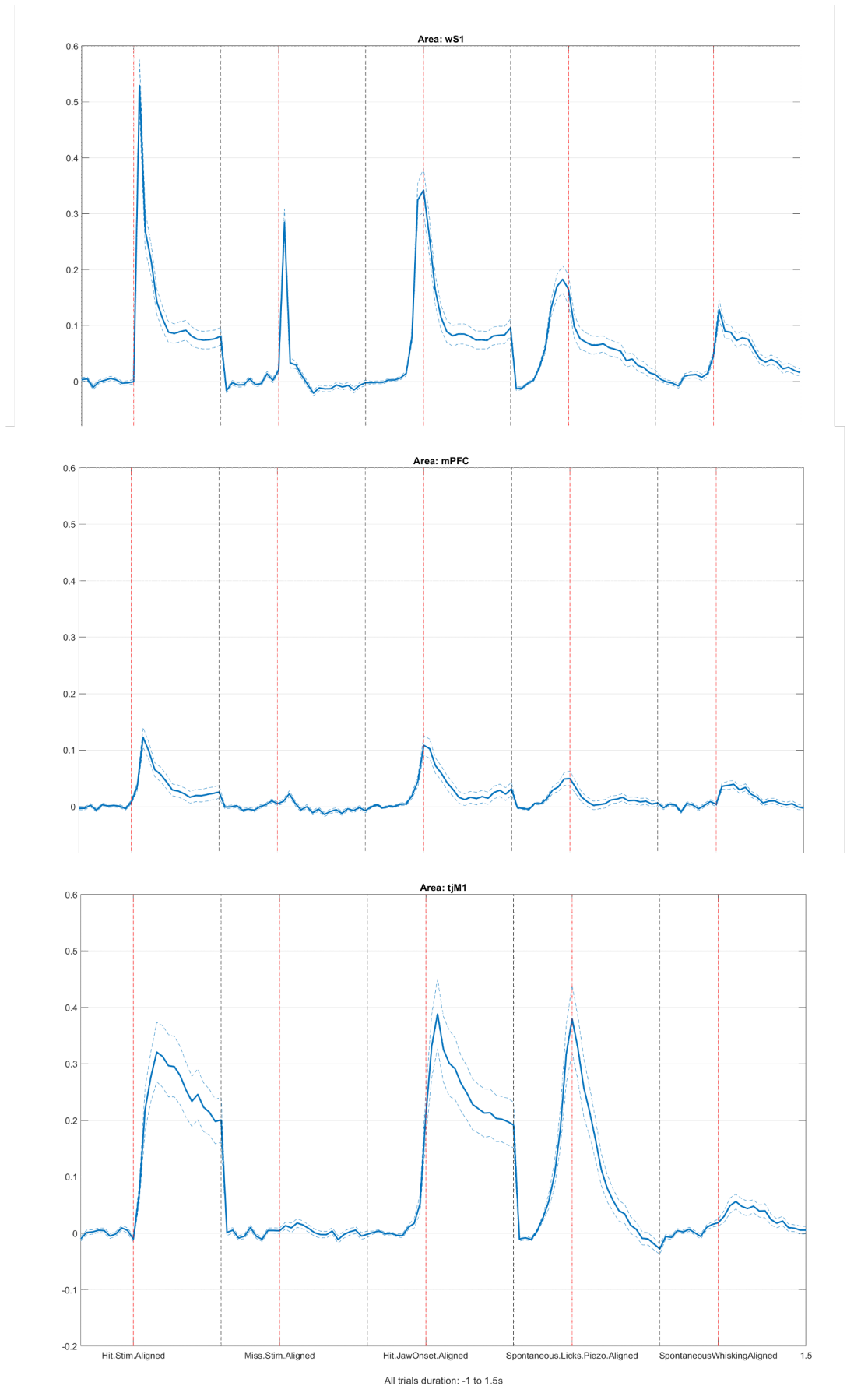


Figure 8: Grand average PSTH of areas wS1, mPFC, tJM1

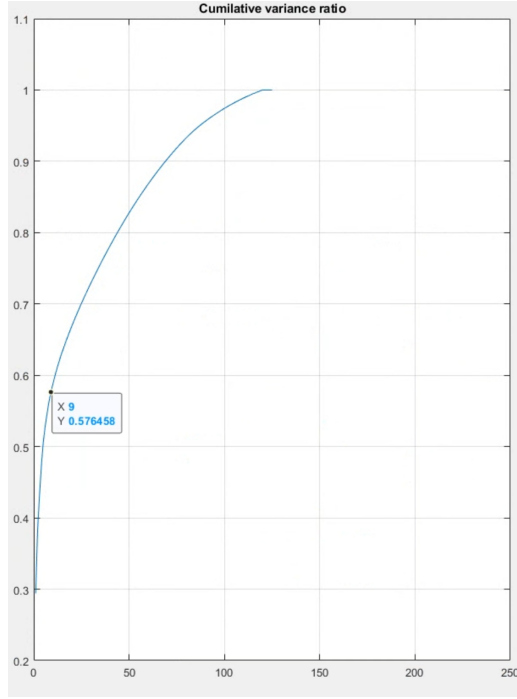


Figure 9: Selection of the number of principal components

By normalizing the data, the weight of distinct components was equalized, resulting in one variance for each component ($X' \in R^{1598 \times 9}$).

Next, spectral embedding was used to identify non-convex and more complicated clusters [1, 51]. To do this, the similarity matrix $S \in R^{1598 \times 1598}$ was calculated, whose element at row i and column j measures the similarity between x_i' and x_j' as

$$s_{ij} = \exp\left(-\frac{\|x_i' - x_j'\|_2^2}{2\sigma^2}\right) \in [0, 1],$$

where σ is a free parameter that determines how local similarity is measured in the feature space. σ was calibrated by setting the average similarity value at 0.5 (the tuned value for σ is 0.135)(Figure 10).

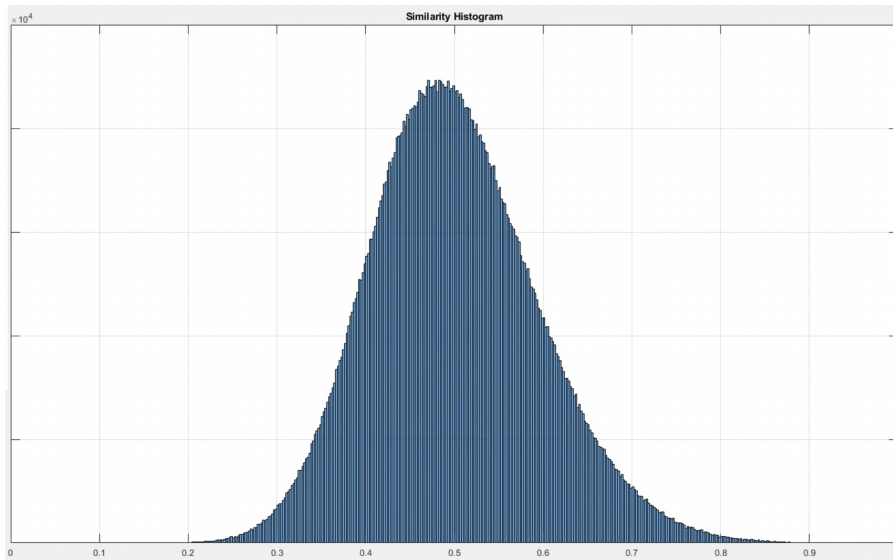


Figure 10: Distribution of the elements of the similarity matrix. Mean is set equal to 0.5.

Then, the normalized Laplacian matrix was constructed using the formula

$$L = I - D^{-0.5}WD^{-0.5},$$

where I is the identity matrix and D is the diagonal degree matrix defined as $\text{diag}(\{\sum_{k=1}^{1598} s_{ik}\}_{i=1}^{1598})$. The transformed features are rather abstract and computed as the eigenvectors of L . Notably, the new feature space is a non-linearly converted version of the PCA space, which itself is a linearly transformed version of the original firing rate space. Such a transformation is believed to naturally separate data points which are clustered together [1, 51]. Using the elbow approach on the eigenvalues of matrix L (i.e., locating the sharp transition in the derivative of sorted eigenvalues), (after omitting the very first eigenvector) the first 8 eigenvectors of matrix L were considered as representative features, resulting in matrix $\tilde{X} \in R^{1598 \times 8}$ (Figure 11). For example, neurons in the 1st 3 dimensions of the spectral space are shown (Figure 12).

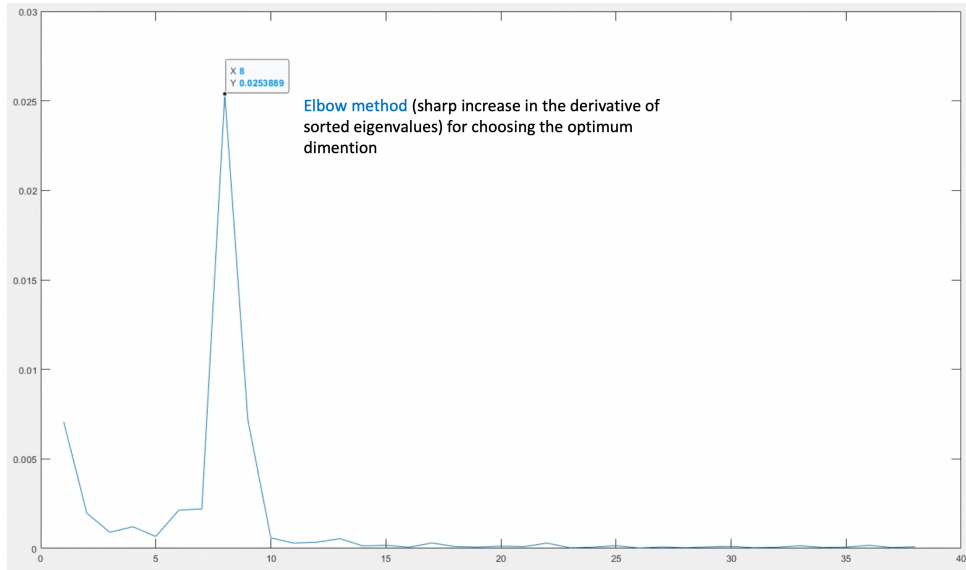


Figure 11: Selection of the optimum number of clusters in spectral embedding using elbow method

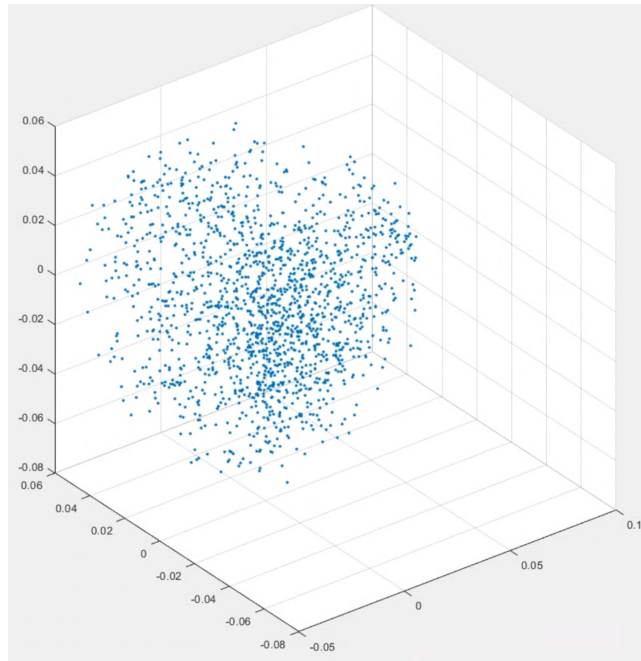


Figure 12: Neurons in the 1st 3 dimensions of the spectral space

Using a Gaussian Mixture Model (GMM), neurons were clustered based on the resulting matrix \tilde{X} . The approach assumes that the underlying data distribution is a combination of K Gaussians with means $\{\mu_1, \dots, \mu_k\}$, diagonal covariance matrices $\{\Sigma_1, \dots, \Sigma_k\}$, and weights $\{\rho_1, \dots, \rho_k\}$. The parameters of this mixture model were computed using the expected maximization (EM) approach for a given K [9]. To do this, the 'fitgmdist' function in MATLAB (Mathworks) was utilized with 1,000 maximum iterations, 0 regularization value, 5000 replicates, and a diagonal covariance matrix constraint. This generates a GMM in which the principal axes of the Gaussians are parallel to the axes of the feature space, providing greater flexibility than the k-means approach while preserving a limited number of fitting parameters. The number of clusters was then chosen ($k = 17$) by minimizing the Bayesian information criterion (BIC) (Figure 13). It is a penalized likelihood term defined as $-2\log(L) + M\log(n)$, where $\log(L)$ is the data's negative log-likelihood, M is the number of GMM parameters, and n is the number of observations. The first term rewards models with strong fit, whereas the second term penalizes models with greater complexity. The BIC score was calculated by the 'fitgmdist' function. Using the fitted parameters, each neuron was assigned a cluster index $k_i \in \{1, \dots, 17\}$ corresponding to the Gaussian distribution to which it most likely belongs. The output of the GMM stage was the vector $K \in \{1, \dots, 17\}^{1598}$ holding the neuron cluster indexes (Figure 6 and 17).

Clusters were sorted according to their onset latency (Figure 14). To do this, first, the average firing rate of neurons belonging to the same cluster were computed, then the mean standard deviation of the baseline is calculated and multiplied to small (10) and large threshold (20) factors to obtain small and large threshold. Threshold factors are obtained manually based on observation of sorting by a neuroscience expert. The first time bin after stimulus which exceeds large threshold is detected (green dot) and the onset time bin (red dot) is the first one before green dot which is below small threshold. Latency is determined as the difference between onset time bin and the time bin which correspond to time zero (blue dot).

To determine the amount that neurons from various brain regions contribute to each cluster composition, two steps were taken. First, the distribution of neurons within each cluster across distinct brain areas was assessed (Figure 19). Weighted proportions were evaluated to account for the disparities in the total number of neurons belonging to each group and brain area. To see how the neurons of a specific area are distributed across clusters, the same calculation of Figure 19 has been done with difference of normalization to the number of clusters instead of the number of areas (Figure 20).

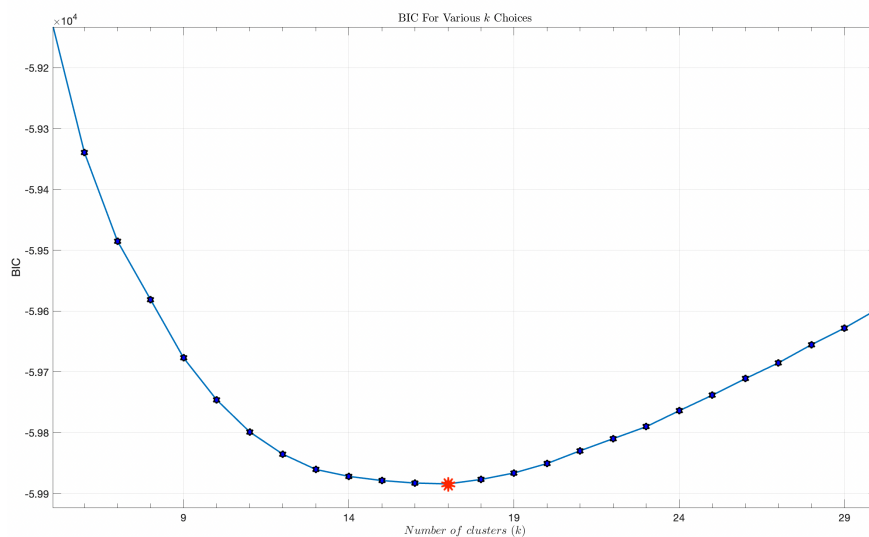


Figure 13: Determination of the number of clusters. Number of optimal clusters ($k=17$) was determined as the minimum of the Bayesian information criterion (BIC) curve.

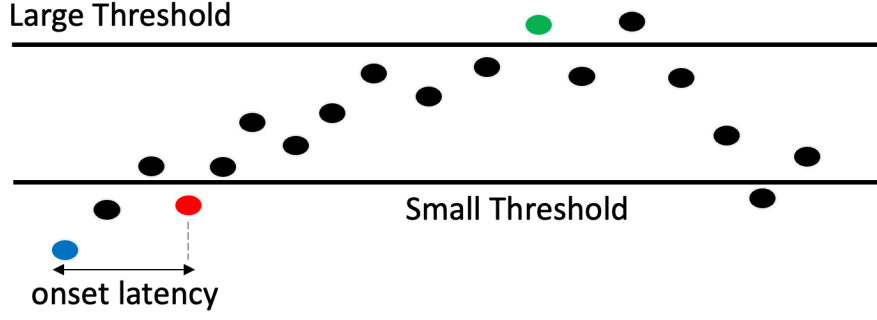


Figure 14: Onset latency determination. The blue and red dot correspond to time zero and the detected onset time bin, respectively. Onset latency is determined as the absolute difference between them.

Finally, a "distribution index" (Figure 18) that measures the dispersion of each cluster across several brain areas was established. The total variation distance between the weighted distribution of neurons was calculated in each cluster across three brain regions and the uniform distribution for this purpose:

$$TV_k = \frac{1}{2} \sum_a \left| \rho_{k,a} - \frac{1}{3} \right|,$$

Where $\rho_{k,a}$ is the weighted proportion of cluster k neurons that belong to region a. Note that $\rho_{k,a}$ has been normalized with respect to areas, i.e., $\sum_a \rho_{k,a} = 1$. The distance TV_k has a minimum value of 0 when the neurons of cluster k are dispersed uniformly across all brain regions and a maximum value of $\frac{2}{3}$ when all neurons of cluster k belong to a single brain region. To scale this value between zero and one, a distribution index was constructed D_k for each cluster k as follows:

$$D_k = 1 - \frac{3}{2} TV_k \in [0, 1],$$

$D_k = 1$ implies that cluster k is uniformly distributed throughout brain regions, while $D_k = 0$ indicates that cluster k is concentrated in a single brain region.

2.8. Interareal connectivity analysis on delayed response neuronal (spikes) data

Utilizing the subset of sessions with simultaneous paired recordings from whisker sensory and motor cortices, the changes in the coordination of interareal wS(1,2)->wM(1,2) neural activity across learning were examined using two distinct techniques.

2.8.1 Pearson correlation

First, the Pearson correlation was determined between trial-by-trial whisker-evoked responses in pairs of individual neurons recorded from wS1/wS2 (5 to 55 ms after whisker onset) and wM1/wM2 (10 to 90 ms after whisker onset) (Figure 29). For the pair-wise correlation analysis, only neurons within the analysis windows whose average firing rate was greater than 2.5 Hz were examined. Similarly, the Pearson correlation between the trial-by-trial average population responses in the same task epochs between pairs of simultaneously recorded areas was calculated (Figure 31A).

2.8.2 Spike Time Tiling Coefficient

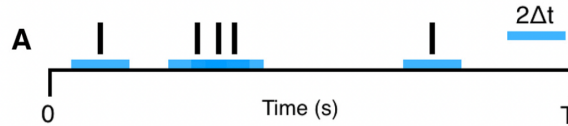
The STTC technique [5] was utilized as a second measure of pair-wise correlation, which is hypothesized to be insensitive to firing rate. The STTC was calculated during a 1-second window centered on the whisker stimulus (Figure 31B) and was defined for spike trains A and B as

$$STTC = \frac{1}{2} \left(\frac{P_A - T_B}{1 - P_A T_B} + \frac{P_B - T_A}{1 - P_B T_A} \right),$$

where P_A and P_B are the proportion of spikes from A falling within $\pm\Delta t$ (± 10 ms) of a spike in B and vice versa and T_A and T_B are the proportion of the total recording time that falls within $\pm\Delta t$ of a spike from B or A, respectively (Figure 15).

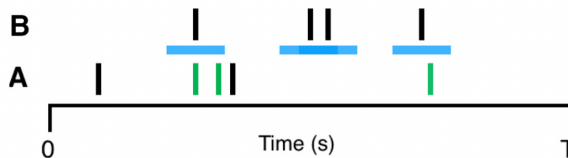
Spike Time Tiling Coefficient - STTC

T_A : the proportion of total recording time which lies within $\pm\Delta t$ of any spike from A. **T_B** calculated similarly.



T_A is given by the fraction of the total recording time (black) which is covered (tiled) by blue bars. Here T_A is 1/3.

P_A : the proportion of spikes from A which lie within $\pm\Delta t$ of any spike from B. **P_B** calculated similarly.



P_A is the number of green spikes in A (3) divided by the total number of spikes in A (5). Here P_A is 3/5.

Figure 15: Diagram illustrating the spike time tiling coefficient computation. P_A , P_B , T_A , and T_B are the four parameters required to determine the spike time tiling coefficient. Δt is the only free parameter. Values and scales are only for illustrative purposes. Adapted from [5].

2.8.3 Cross-correlograms

In addition, directional functional connectivity from wS1 to wM1 and from wS2 to wM2 was determined using cross-correlograms (CCG) within a 1 second window centered on whisker stimulus (Figure 30, and 31). The CCG was defined as

$$CCG(\tau) = \frac{\frac{1}{M} \sum_{i=1}^M \sum_{t=1}^N \chi_1^i(t) \chi_2^i(t + \tau)}{\theta(\tau) \sqrt{\lambda_1 \lambda_2}},$$

where M is the number of trials, N is the number of bins in the trial, χ_1^i and χ_2^i are the spike trains of the 2 units on trial i, τ is the time lag relative to reference spikes, and λ_1 and λ_2 are the mean firing rates of the reference and target units, respectively. $\theta(\tau)$ is the triangle function that corrects for the overlap of time bins resulting from the sliding window [33]. Within the analysis window, neurons with a firing rate greater than 1 Hz were included in the analysis. Cross-correlograms were corrected by removing a jittered version [41, 44] (Figure 31C) to better capture fast timescale changes related to feedforward connections

$$CCG_{corrected} = CCG - CCG_{jittered}$$

The jittered CCG was generated by averaging 100 resamplings of the original dataset in which spike times inside each 25-ms window were permuted randomly across trials. This technique eliminates stimulus-locked and slow timeframe correlations bigger than the jitter window while maintaining the trial-averaged PSTH and number of spikes each unit [16]. The significant directional link from reference to target neuron was determined for each pair of recorded units if the maximum CCG within time lags between 0 and 10 ms was greater than the 6-fold standard deviation of the jitter-corrected CCG flanks (between ± 50 to 100 ms). For both analytical methods, in wS1/wS2, we concentrated only on RS units, which are known to have long-range projections. In wM1/wM2, correlations and directional connectivity were evaluated independently for RS and FS units.

2.9. Statistics

Data are represented as mean \pm SEM unless otherwise noted. The Wilcoxon signed-rank test was used to determine statistical significance for paired comparisons, whereas the Wilcoxon rank-sum test was employed for unpaired comparisons (MATLAB implementations). P-values are adjusted in clustering and connectivity analysis to accommodate multiple comparisons by Bonferroni and FDR corrections, respectively.

3. Results

3.1. Clustering analysis of neural data

Single neurons encode distinct components of task execution, including whisker sensory processing, lick preparation by decision, and lick execution (Figure 16). Assuming that neurons with similar firing dynamics perform similar processing, it is advantageous to identify these temporal patterns and determine if a given pattern is localized to a specific brain region or widespread throughout the brain. Unsupervised clustering of neurons was performed on the basis of their temporal firing pattern across several trial types (Hit, Miss, Spontaneous licks, and whisking) by combining neurons from different brain regions. Clustering based on the Gaussian mixture model (GMM) produced 17 groups of neurons (Figure 17), sorted by their onset latency. Next, a "distribution index" was calculated that measures the composition of clusters inside versus between areas (Figure 18). The low distribution index for wS1 clusters (1, 2, 3), tJM1 clusters (5, 8, 11), and mPFC clusters (6, 17) indicates their limited distribution in specific brain areas. In contrast, the dispersion index was high for the other clusters, indicating that these clusters are widely distributed across brain regions.

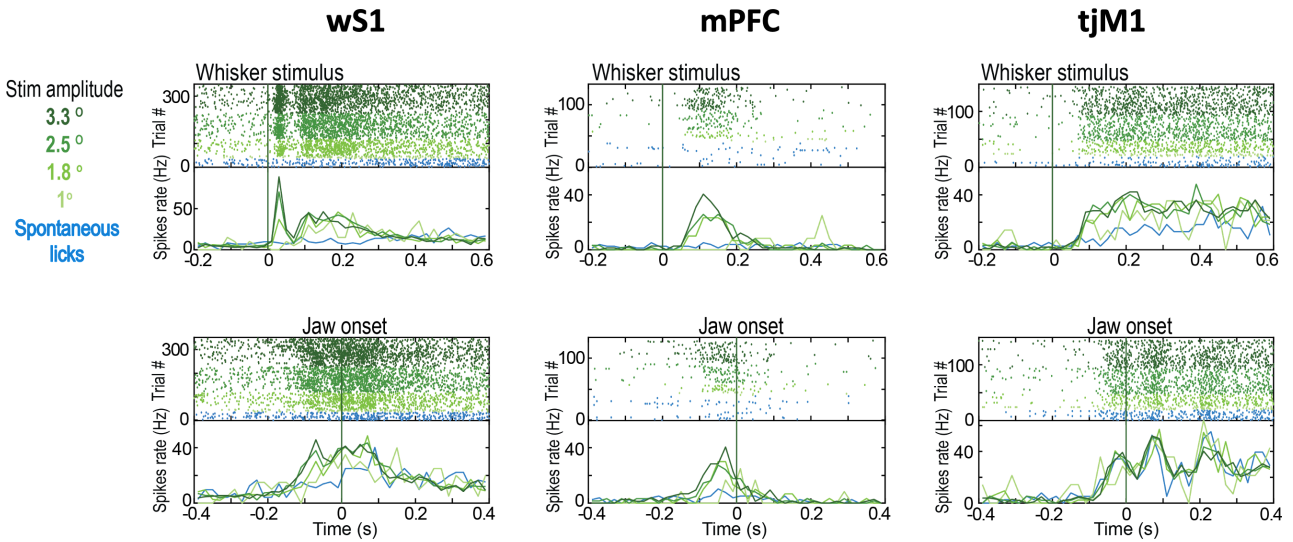


Figure 16: Example neurons. Raster plots and peristimulus time histograms (PSTHs) for three representative units in wS1 (encoding whisker), mPFC, and tJM1 (encoding licking).

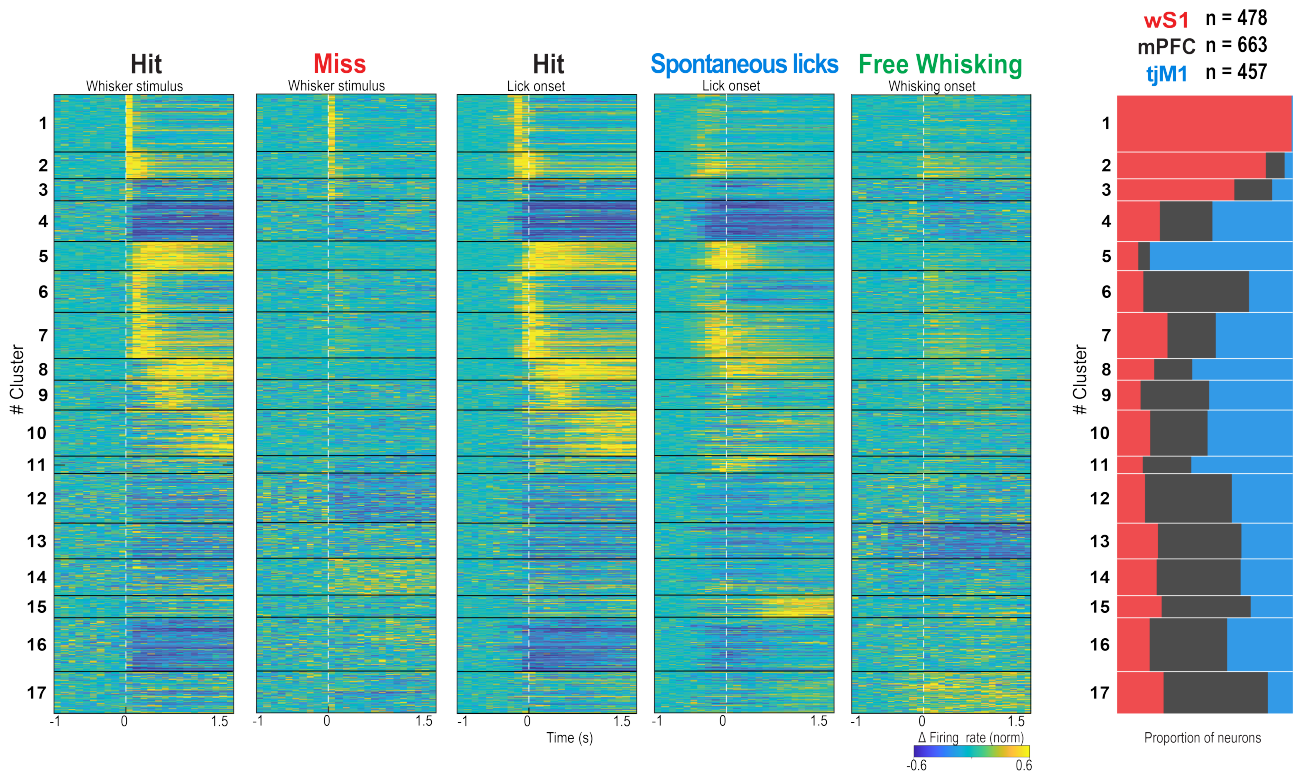


Figure 17: PSTH of all neurons clustered and weighted proportion of neurons within each cluster belonging to different brain regions.

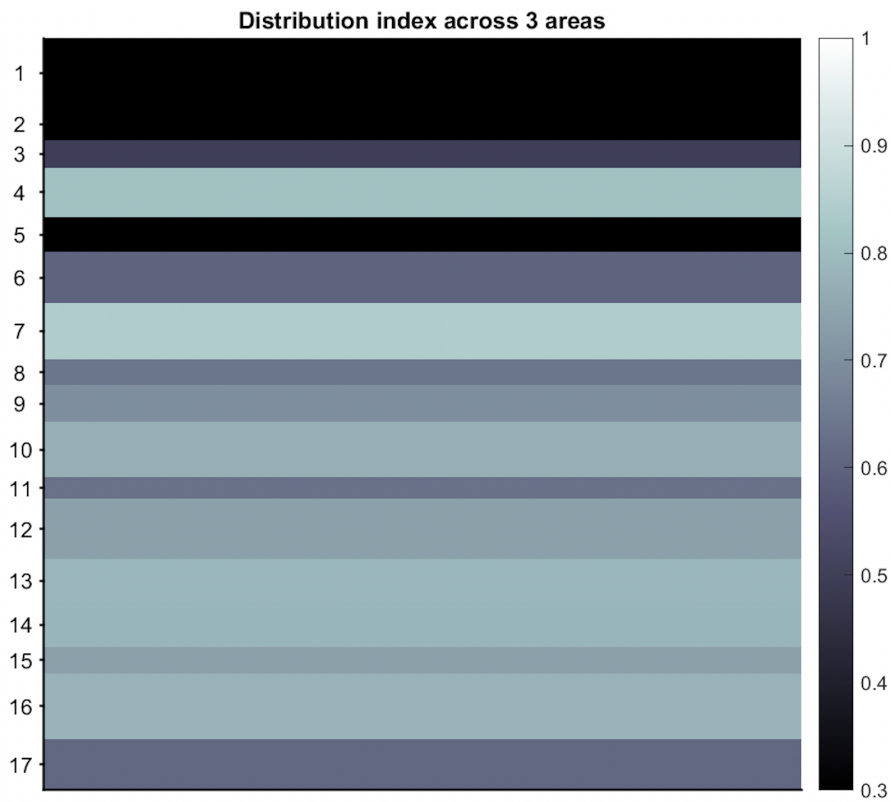


Figure 18: Distribution index. To calculate distribution index for each cluster, the probability distribution of the area composition was compared to a uniform distribution, and an index between 0 (localized in one area) to 1 (uniformly distributed) was defined. Values are corrected for different sample size in different areas.

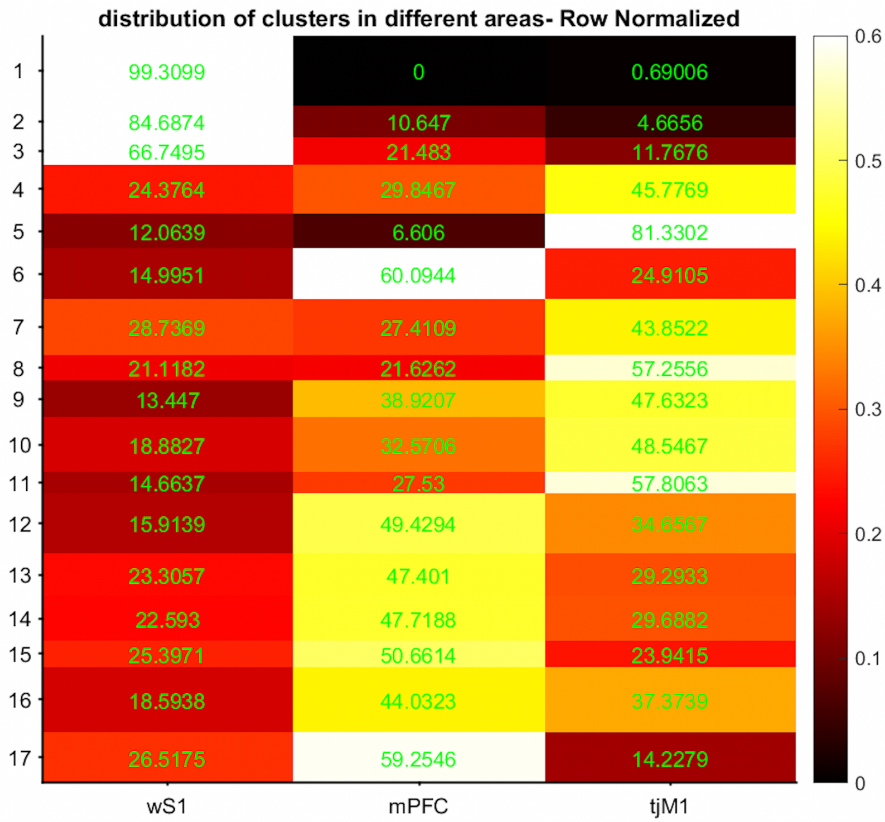


Figure 19: Composition of clusters. Weighted proportion of neurons within each cluster belonging to different brain regions

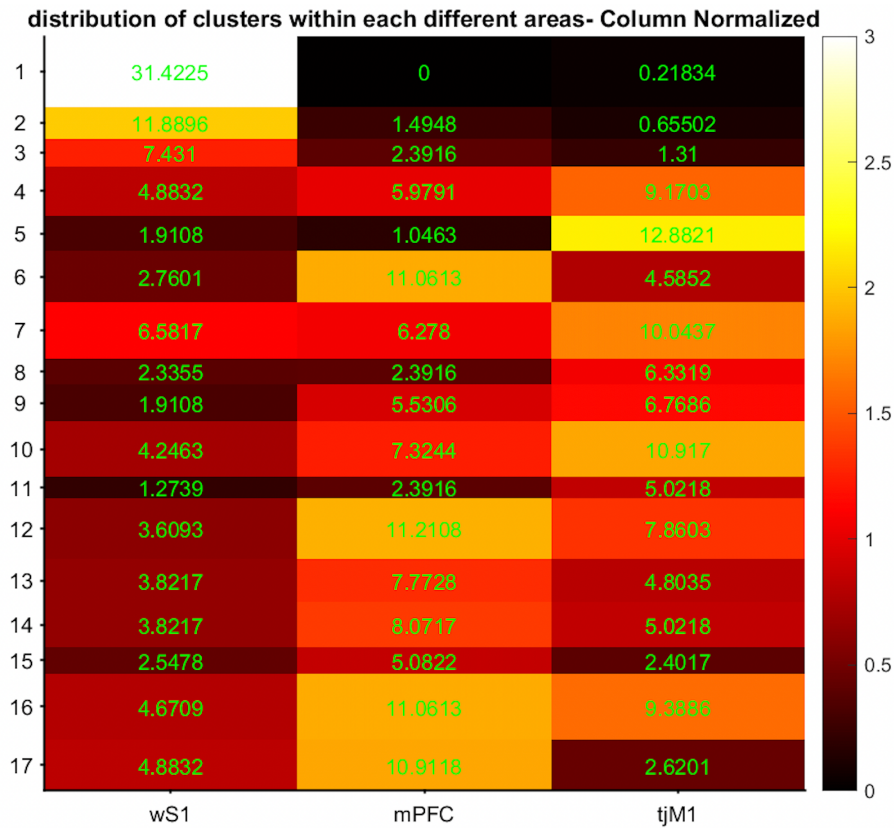


Figure 20: Composition of areas. Weighted proportion of neurons within each area belonging to different clusters

The neuronal clustering revealed some patterns of activity: (1) a rapid and transient increase in neuronal activity following the whisker stimulus (clusters 1–3), which was predominantly represented in wS1; (2) both inhibition (clusters 4) and excitation (cluster 5,7-11) mainly in tjM1; and (3) complex behaviours mainly in mPFC (cluster 6,12-17). cluster 1 and 2 are mostly composed by wS1 neurons, cluster 5 by tjM1 neurons, and cluster 6 by mPFC neurons indicating that there are specific patterns related to a specific area. Strikingly, the majority of clusters are represented by neurons of all three areas pointing to a distributed information coding and that similar neuronal responses can be found in all three areas.

3.1.1 How sensory information is represented by neuronal activity?

To understand pure sensory coding, trials where the mouse receives sensory stimuli but does not lick (Miss trials) were selected and compared. Comparing wS1, mPFC, and tjM1 in terms of coding the sensory stimulus and stimulus amplitude by fitting a linear regression (Pearson correlation) on the response of neurons to various stimulus amplitudes demonstrates that wS1 contains a large number of sensory neurons, whereas mPFC and tjM1 contain a small number of sensory neurons (Figure 21). In figure 22, grand average PSTH of most representative clusters of wS1 is shown. We have sensory neurons in clusters 1, 2, and 3 with the major contribution of wS1 however, it is evident that mPFC is the second contributor in the composition of clusters 2 and 3 indicating the existence of sensory neurons in mPFC. Considering hit trials, there is a secondary lasting excitation in cluster 2 and a secondary lasting inhibition in cluster 3 compared to cluster 1, which is 99 percent wS1.

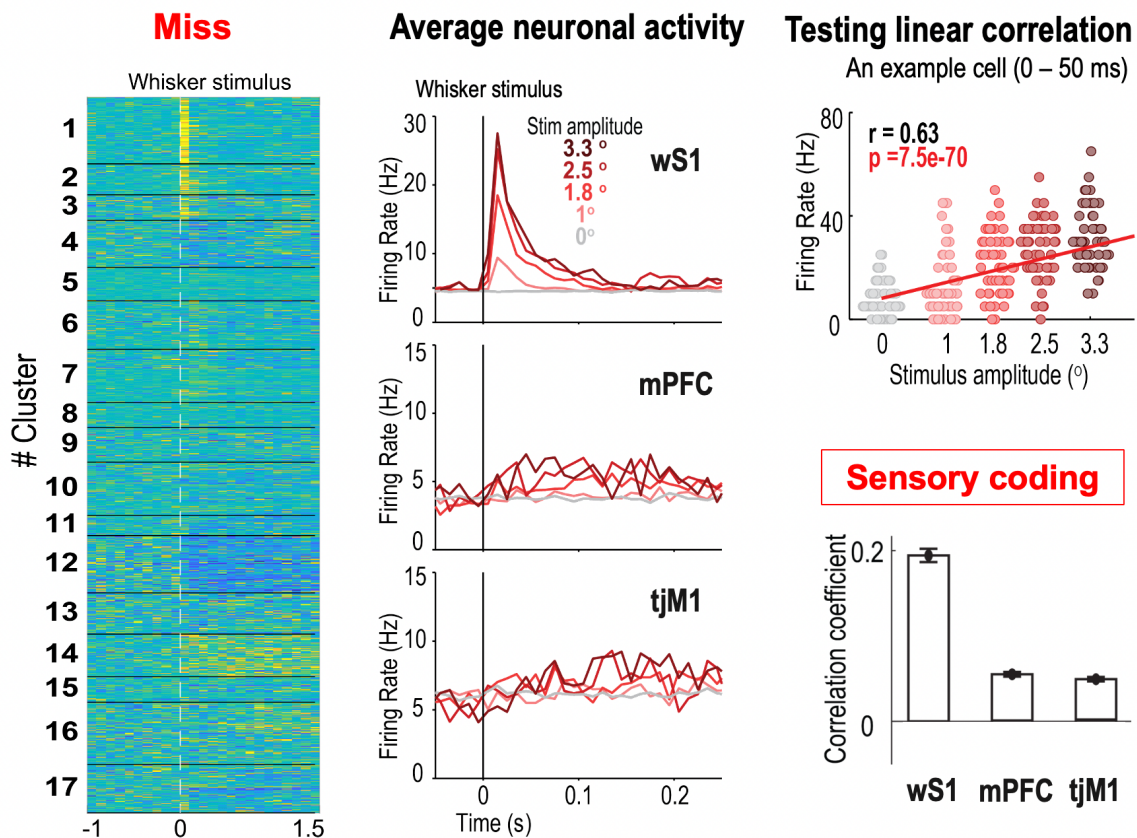


Figure 21: Left column: Miss trials of different neurons in associated clusters. Middle column: Average neuronal activity of the three areas to different stimulus amplitudes. Right column up: fitting linear regression on an example neurons response. Right column down: Average positive Pearson correlation coefficient for the three areas.

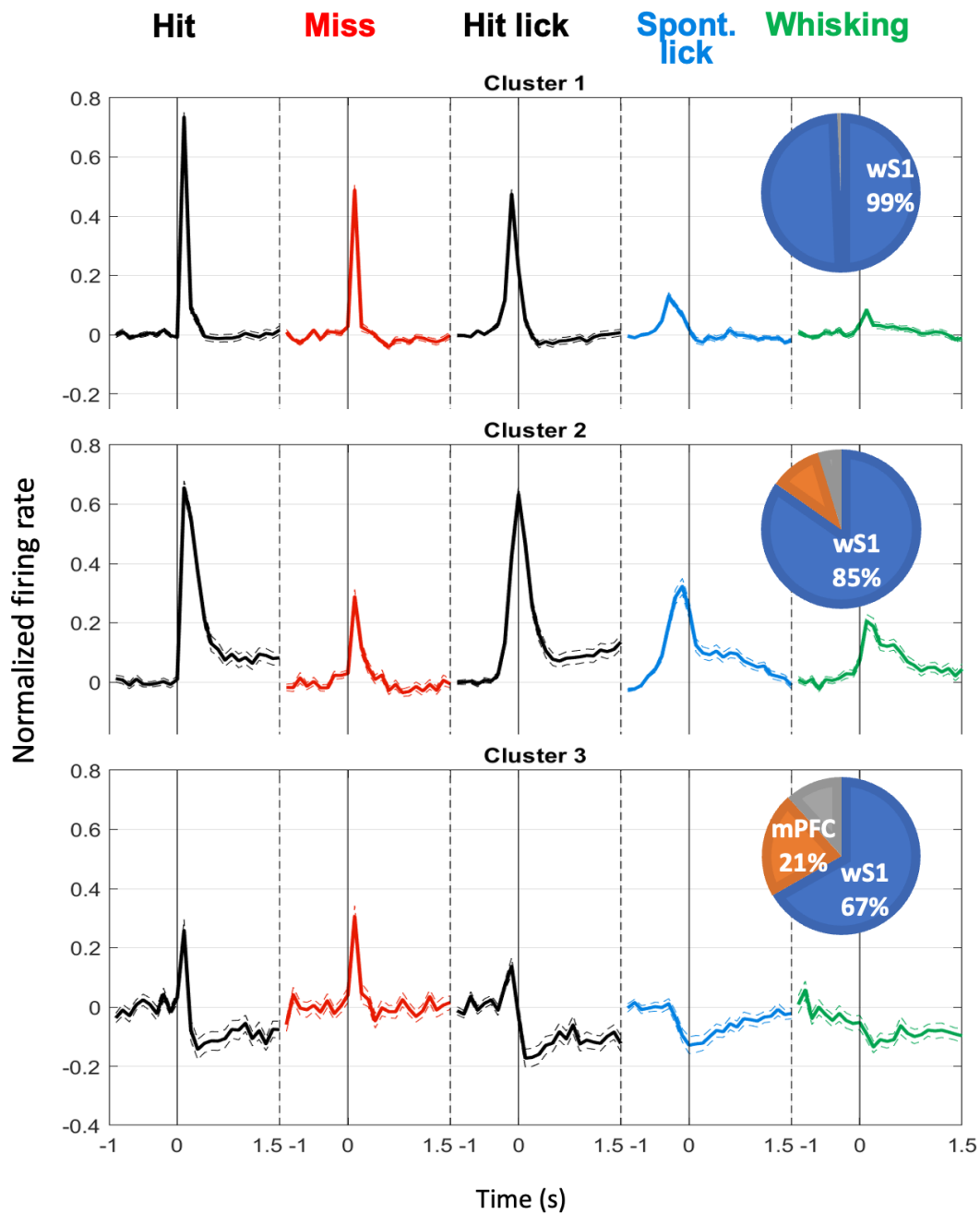


Figure 22: Clusters 1-3. Most representative clusters of wS1.

3.1.2 How motor information is represented by neuronal activity?

To evaluate pure motor coding, movement-related activity where no sensory stimulus was present (Spontaneous licks trials) was chosen. Comparing wS1, mPFC, and tjM1 in terms of encoding the phase of the jaw movement based on the response of neurons reveals that tjM1 has a big number of phase coding related neurons while wS1 and mPFC contain a small number (Figure 23). In figure 24, grand average PSTH of most representative clusters of tjM1 is shown. As demonstrated in the figure below, jaw opening-related clusters which contain mainly motor related neurons are widespread across the areas; however, cluster 5 is quite specific to tjM1 and there is not any activity in miss trials.

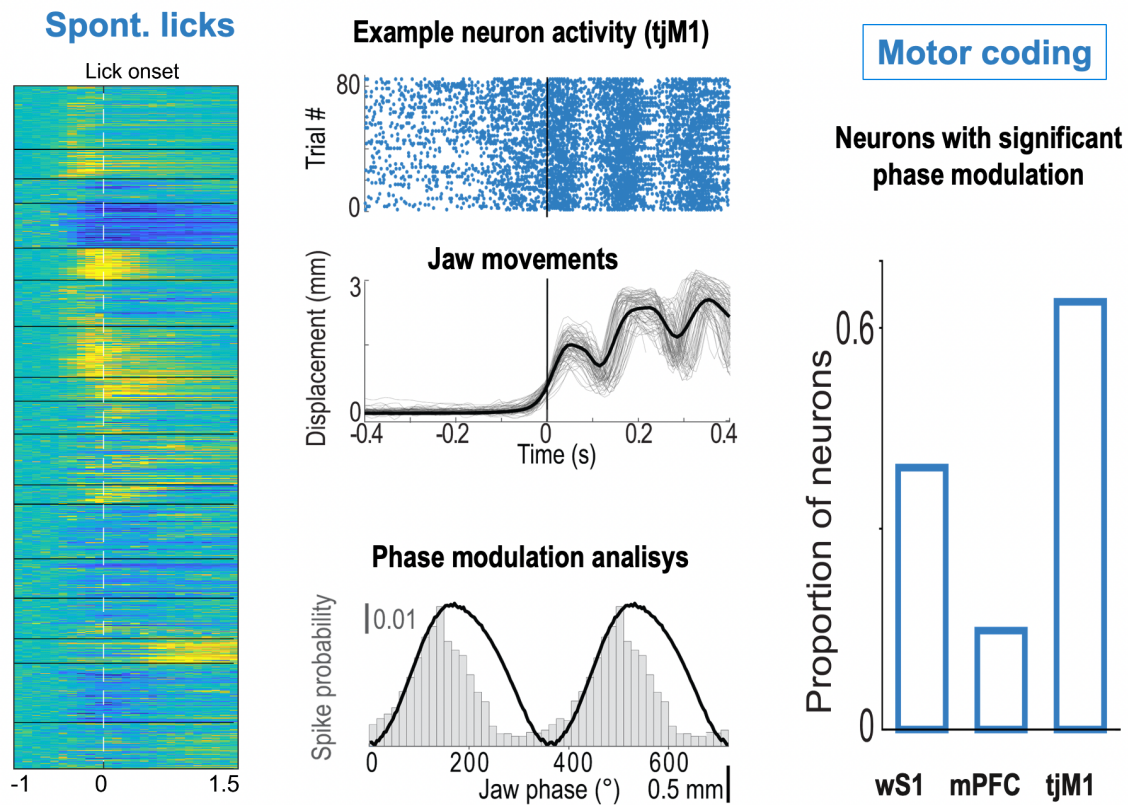


Figure 23: Left column: Spontaneous licks trials of different neurons in associated clusters. Middle column up: Raster plot of an example neuron of tJM1 and average jaw movement in spontaneous licks trials. Middle column down: Spiking probability of the exemplified neuron with respect to phase of the jaw movement. Right column: Proportion of the neurons from the three areas which are significantly phase modulated.

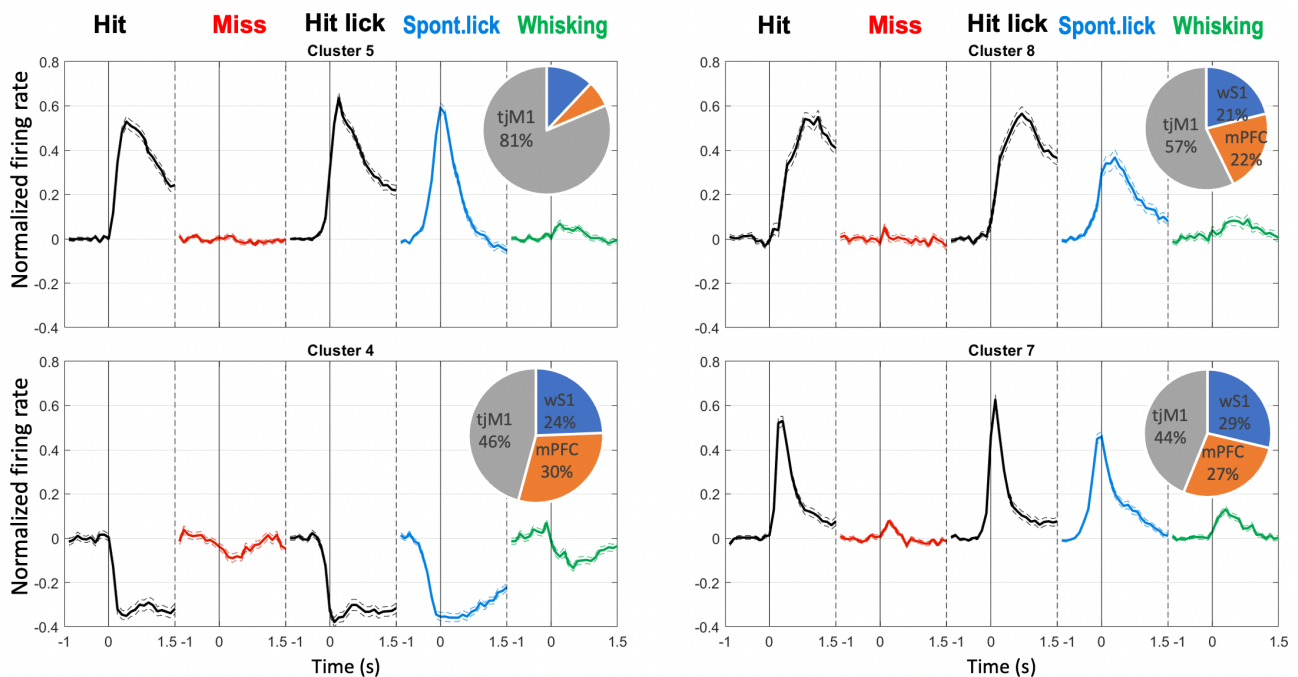


Figure 24: Clusters 4, 5, 7, 8. Most representative clusters of tJM1.

3.1.3 How choice information is represented by neuronal activity?

For the Identification of choice or decision neurons, they should exhibit activity in hit trials but not in miss and spontaneous licking trials as the decision is defined to lick the spout in presence of a whisker stimulus. Choice neurons are distributed across areas but more in mPFC (Figure 25). Despite having minor activity in miss and spontaneous lick trials, cluster 6 is the closest to the definition of choice neurons between all clusters and choice neurons are sub-group of this cluster (Figure 26).

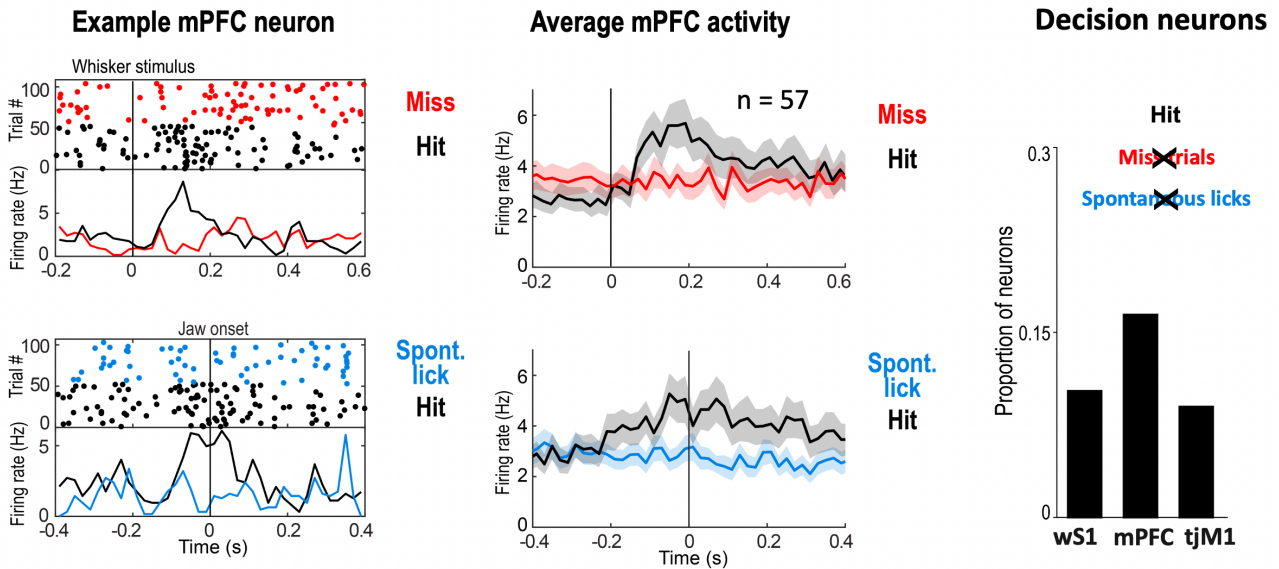


Figure 25: Left column: Raster plot and PSTH of an example choice neuron of mPFC in hit vs miss and hit vs spontaneous licks trials. Middle column: Grand average PSTH of choice neurons of mPFC discovered via direct observation in hit vs miss and hit vs spontaneous licks trials. Right column: Proportion of the choice neurons from the three areas.

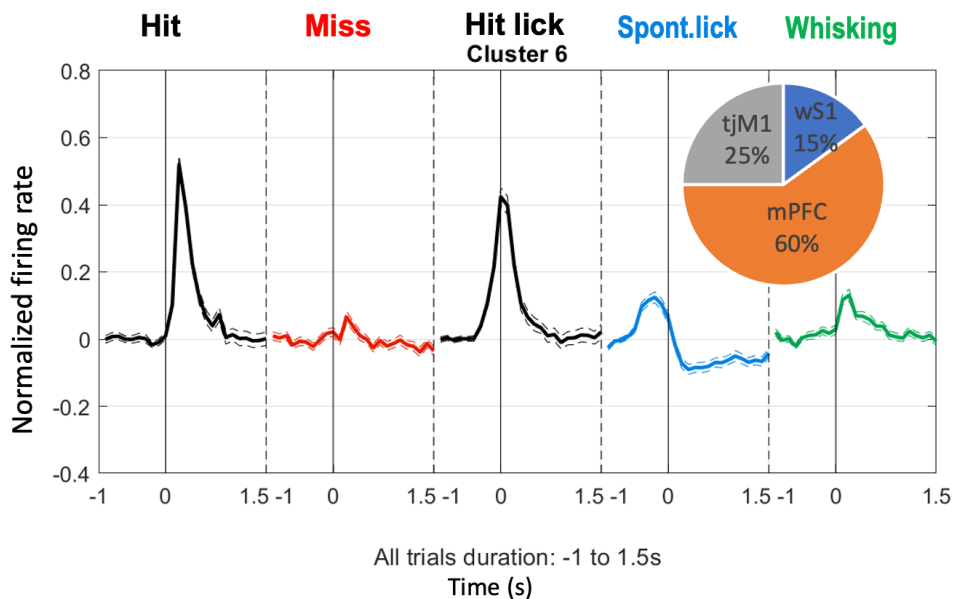


Figure 26: Cluster 6. The most representative cluster of mPFC.

3.1.4 What else is represented in mPFC?

Two of the clusters, 15 and 14, display an intriguing pattern of activity that may indicate a role for the areas, most notably the mPFC, in the generation of teaching signals for learning by error (Figure 27). Cluster 15 demonstrates that there is a maximal activity in spontaneous licks that do not match motor activity since it is absent in hit trials and may signal the absence of the reward despite licking (reward expectation). Cluster 14 reveals that there is a maximal activity when the reward is missed and may signal the mice not doing the task correctly.

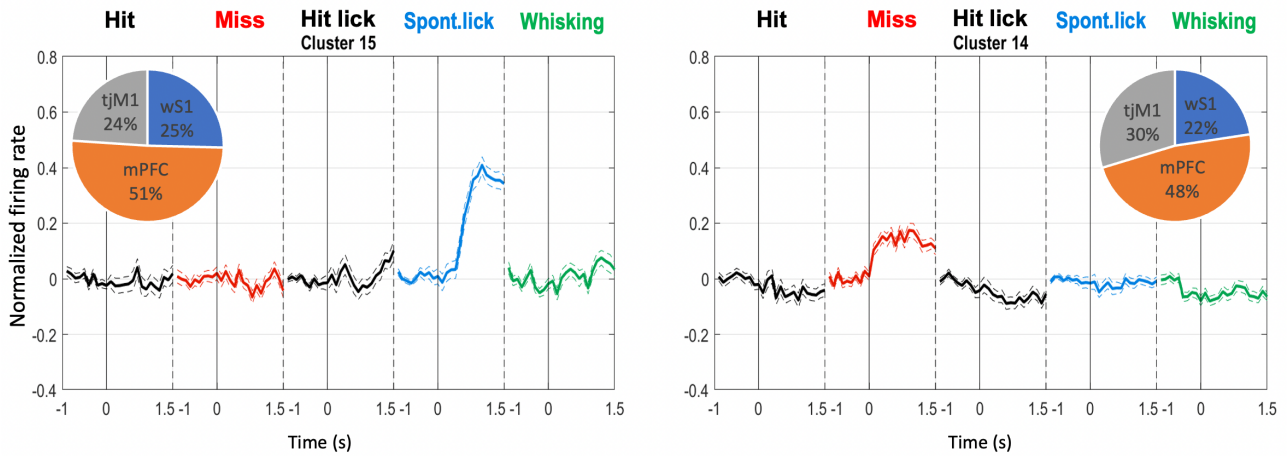


Figure 27: Clusters 14 and 15. Error (teaching) signal in mPFC.

3.2. Connectivity analysis of neural data (wS(1,2) -> wM(1,2))

It has been found out that wS1 innervates frontal cortex with a column of axons in a cortical area that is called wM1. Similarly, wS2 axons project to frontal cortex in a columnar manner in a region labeled as wM2. The location of wM2 seemed more anterior than that of wM1 which is located at 1.0 mm anterior and 1.0 mm lateral to bregma, but wM2 was located at 1.9 mm anterior and 1.2 mm lateral to bregma. Therefore, the primary and secondary somatosensory cortices project onto the frontal cortex.

Next, the effects of task learning on whisker deflection-evoked neuronal activity in wM1 and wM2 were examined. RS (putative excitatory) and FS (putative inhibitory) neurons in both wM1 and wM2 and in both Novice (untrained) and Expert (trained) mice showed obvious fast sensory-evoked modulation. However, RS and FS neurons in these two adjacent cortical regions altered their activity patterns differently during learning. In wM1, RS units had a smaller whisker-evoked response in Expert mice than in Novice mice (Novice: 1.8 ± 3.0 Hz, 147 units recorded in 7 mice, Expert: 0.9 ± 3.9 Hz, 452 units recorded in 11 mice; nonparametric permutation test, $p = 0.002$) (Figure 28A), whereas FS units had a greater response in Expert mice (Novice: 3.1 ± 3.6 Hz, 66 units recorded in 7 mice, Expert: 7.3 ± 16.9 Hz, 134 units recorded in 11 mice; nonparametric permutation test, $p = 0.0008$) (Figure 28B). The ratio of RS to FS firing in wM1 is therefore strongly changed in Expert mice in favor of FS units. In contrast, it was noticed that neuronal activity in wM2 was altered in a significantly different way during learning than in wM1. In wM2, whisker deflection evoked an increased AP firing in RS units of Expert mice compared to Novice mice (Novice: 1.0 ± 2.2 Hz, 244 units recorded in 7 mice, Expert: 1.5 ± 4.5 Hz, 401 units recorded in 10 mice; nonparametric permutation test, $p = 0.016$) (Figure 28C), but a decreased firing of FS units (Novice: 4.5 ± 6.8 Hz, 57 units recorded in 7 mice, Expert: 2.7 ± 3.9 Hz, 107 units recorded in 10 mice; nonparametric permutation test, $p = 0.021$) (Figure 28D). The balance of RS to FS unit activity in wM2 is therefore enhanced in favor of RS units across task learning.

To examine how the coordination between sensory and motor cortices changed throughout the course of learning, interareal interactions were assessed among wS1->wM1 and wS2->wM2 in the subset of sessions in which simultaneous paired recordings from these regions were collected (Figure 29 and Figure 30). Averaged over individual pairs of neurons, trial-by-trial correlation between evoked activity of wS2-RS units with wM2-RS units increased across learning (Novice: 876 neuron pairs recorded in 6 mice, Expert: 583 neuron pairs recorded in 3 mice; Wilcoxon rank-sum test, $p = 0.039$) while it decreased between wS2-RS units and wM2-FS units (Novice: 343 neuron pairs recorded in 6 mice, Expert: 209 neuron pairs recorded in 3 mice; Wilcoxon rank-sum test, $p = 2.9 \times 10^{-4}$). These apparent changes in correlations may be influenced by variations in firing rates caused by learning. Despite the fact that the activity of wM1 FS units increased with learning, the correlation between wS1-RS units and wM1-FS units did not alter considerably, nor did the connection between wS1-RS units and wM1-RS units. As a further control, interareal pairwise correlations utilizing the spike time tiling coefficient (STTC) approach were assessed [5], which is believed to be insensitive to firing rate (Figure 31B). Using STTC analysis, the only significant increase in correlation across learning was found between wS2-RS and wM2-RS units (Novice: 3,482 neuron pairs recorded in 6 mice; expert: 2,461 neuron pairs recorded in 3 mice; Wilcoxon rank-sum test, $p = 4.7 \times 10^{-11}$). Trial-by-trial correlation of the population response showed similar patterns of change across learning in both area pairs as those observed in pair-wise correlation changes (Figure 31A). To further analyze changes in functional connectivity, the amount of directional connections (putative direct monosynaptic connections) were determined based on short-latency sharp peaks in the cross-correlograms between pairs of neurons from the whisker sensory and whisker motor cortices (Figure 30 and 31C). The number of linkages between wS2-RS units and wM2-RS units increased significantly as learning progressed (Novice: 3 connections out of 1,077 pairings in 6 mice; expert: 17 out of 1,066 pairs in 3 mice; chi-squared proportion test, $p = 0.0032$). These findings show that learning increases the ratio of excitation to inhibition in the sensory-evoked response in wM2, but decreases it in wM1 in favor of inhibition. Increased functional connec-

tivity between wS2 and wM2 may result in increased activity of excitatory neurons in wM2 in answer to learning.

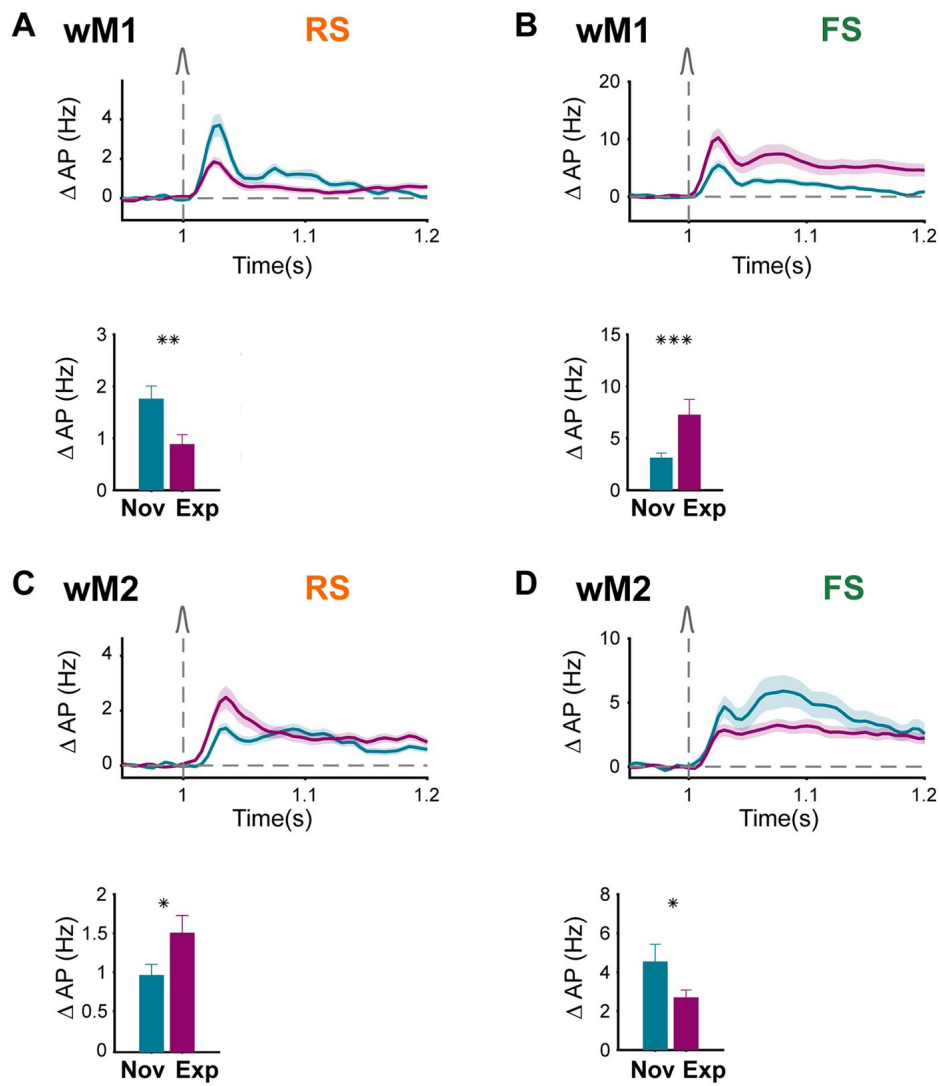


Figure 28: Learning differentially modulated sensory responses of RS and FS neurons in wM1 and wM2 areas. (A) Decrease of whisker response in wM1 RS neurons across learning. Top: baseline-subtracted (50 ms prior to whisker onset) population firing rate (mean \pm SEM) overlaid for Novice mice (147 neurons in 7 mice) and Expert mice (452 neurons in 11 mice). Bottom: Comparison of whisker-evoked response in Novice and Expert mice. Bar plots showing average population firing rate in 10- to 90-ms window (mean \pm SEM) after whisker onset and statistical comparison using nonparametric permutation test (left) (**: $p < 0.01$; *: $p < 0.05$). (B) Increase of whisker response in wM1 FS neurons across learning. Similar to (A) but for wM1 FS neurons in Novice (66 neurons in 7 mice) and Expert mice (134 neurons in 11 mice) (***: $p < 0.001$). (C) Increase of whisker response in wM2 RS neurons across learning. Similar to (A) but for wM2 RS neurons in Novice (244 neurons in 7 mice) and Expert mice (401 neurons in 10 mice). (D) Decrease of whisker response in wM2 FS neurons across learning. Similar to (A) but for wM2 FS neurons in Novice (57 neurons in 7 mice) and Expert mice (107 neurons in 10 mice).

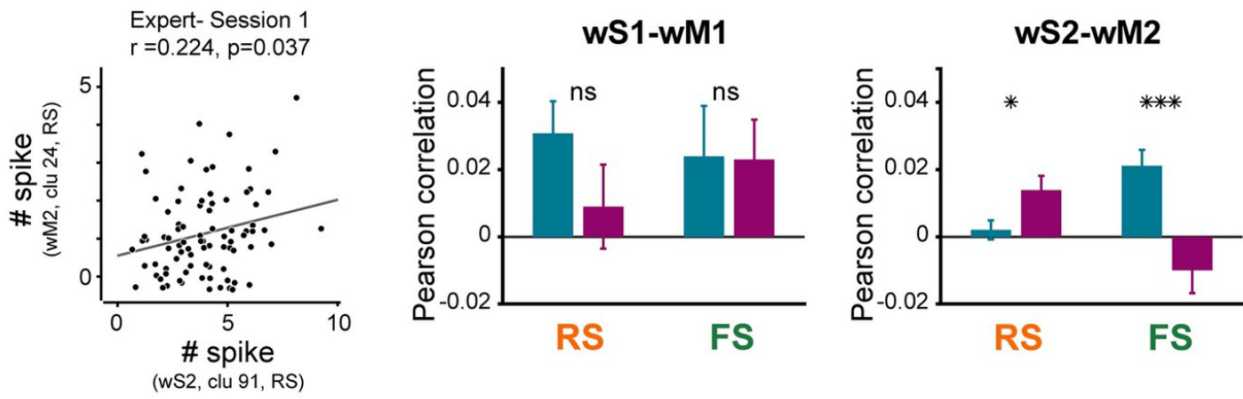


Figure 29: Pair-wise correlation between sensory and motor cortices in Novice and Expert mice. Left: A scatter plot illustrating the trial-by-trial correlation between the whisker-evoked response of a sample pair of neurons in wS2 and wM2. Each circle indicates the neural pair's response in a 1 trial. The circles were slightly jittered for viewing purposes. Gray line: least-squares regression. Middle: Average pair-wise Pearson correlation of wS1-RS units with wM1-RS (110 neuron pairs in 1 Novice mouse, and 68 neuron pairs in 2 Expert mice) and wS1-RS units with wM1-FS units (44 neuron pairs in 1 Novice mouse, and 89 neuron pairs in 2 Expert mice) separately. Right: Average pair-wise Pearson correlation between wS2-RS units and wM2-RS units (876 neuron pairs in 6 Novice mice and 583 neuron pairs in 3 Expert mice) and wS2-RS units and wM2-FS units (343 neuron pairs in 6 Novice mice and 209 neuron pairs in 3 Expert mice). Error bars: SEM. The Wilcoxon rank-sum test was used to compare Novice and Expert statistically (ns: $p \geq 0.05$; *: $p < 0.05$; ***: $p < 0.001$).

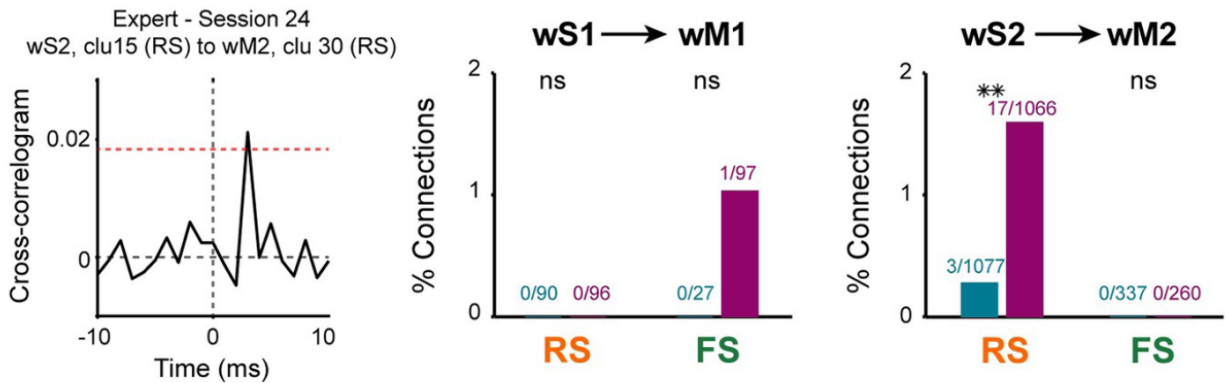


Figure 30: Cross-correlograms are used to determine interareal functional connectivity. Left: Example of a cross-correlogram between two neurons from wS2 and wM2 simultaneously recorded. Red dotted line indicates the threshold for detecting sharp peaks. A directional connection between wS2 and wM2 has been detected due to a threshold crossing between 0 and 10 milliseconds. Middle: Percentage of discovered connections from wS1-RS to wM1-RS and wM1-FS in 1 Novice and 2 Expert mice. Right: Percentage of discovered directional connections from wS2-RS to wM2-RS and wM2-FS units in six novice and three expert mice. The numbers on each bar show the total number of discovered connections and recorded pairs. Using a chi-squared proportion test, the percentages of connections in Novice and Expert were compared (ns: $p \geq 0.05$; **: $p < 0.01$).

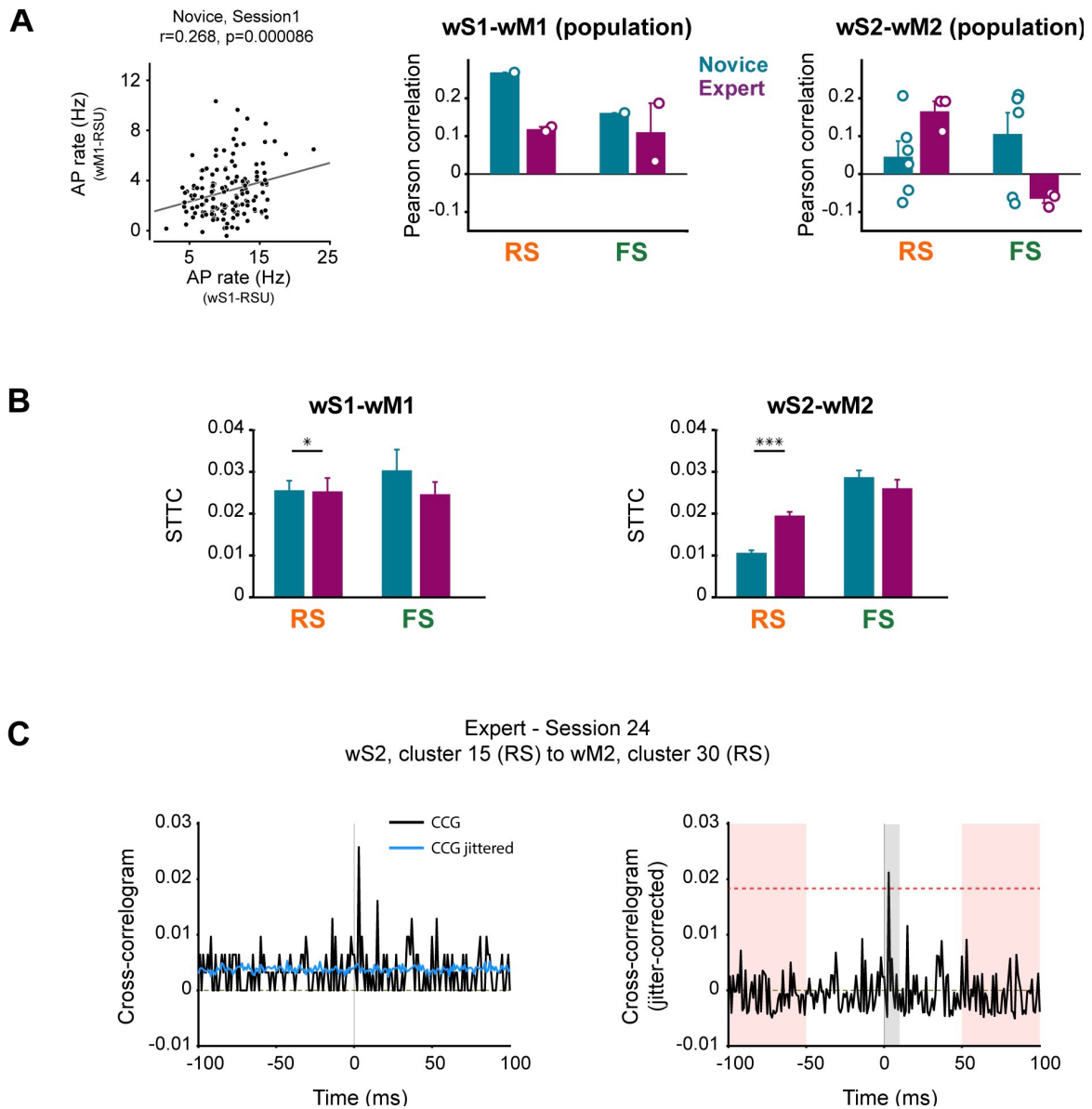


Figure 31: (A) Interareal correlation of population response in Novice and Expert mice. (Left) Scatter plot of the average trial-by-trial population response between wS1-RS units and wM1-RS units for a Novice session. The circles were slightly jittered for viewing purposes. Gray line: least-squares regression. Pearson correlation of trial-by-trial average population response of wS1-RS and wM1-RS and wS1-RS and wM1-FS units (1 Novice and 2 Expert mice). (Right) Pearson correlation of trial-by-trial population average response of wS2-RS vs wM2-RS and wS2-RS versus wM2-FS units (6 Novice and 3 Expert mice). Circles represent separate sessions. Error bars: SEM. (B) Correlation between the sensory and motor cortices of novice and expert mice utilizing the STTC technique. Left: Average pair-wise STTC correlation of wS1-RS units with wM1-RS (308 neuron pairs in 1 Novice mouse and 398 neuron pairings in 2 Expert mice) and wS1-RS units with wM1-FS units (112/139 neuron pairs in 1 Novice mouse and 2 Expert mice, respectively). Right: Average pair-wise Pearson correlation between wS2-RS units and wM2-RS (3,482 neuron pairs in 6 Novice mice and 2,461 neuron pairs in 3 Expert mice) and wS2-RS units and wM2-FS units (821 neuron pairs in 6 Novice mouse, and 532 neuron pairs in 3 Expert mice). Error bars: SEM. The Wilcoxon rank-sum test was used to compare Novice and Expert statistically (ns: $p \geq 0.05$; *: $p 0.05$; ***: $p 0.001$). (C) Example cross-correlogram (CCG) from a pair of neurons simultaneously recorded in wS2 and wM2 of an Expert mouse with a significant connection; similar example pair as in Figure 30, but with CCG from -100 to 100 ms time lags. Jitter correction approach (left) and significant functional connections detection (right). Significant connections were detected if any threshold crossing happened within 0- to 10-ms time lags (gray bar) of the jitter-corrected CCG. Threshold (red dotted line) was defined as 6-fold standard deviation of the jitter-corrected CCG flanks (red bars).

4. Conclusions

To identify functional clusters of neurons (Figure 17), a GMM-based clustering approach was applied to the matrix of contributions of behavioral variables to neural activity. This generates a GMM model with gaussians fitted on the data. To test the fit of the clustering model, we randomized 1,000 times the relative contribution values across behavioural variables. After each iteration of shuffling, the dimension reduction was repeated and log-likelihood was recalculated. The distribution of log-likelihood values for shuffled data (Bonferroni corrected) was then compared to the distribution of log-likelihood values for the PCA applied to the actual data. The number of clusters was decided using the BIC score (Figure 13). The clusters were then analyzed in terms of the distribution of neurons from various regions, and the potential function of each cluster was assessed. Clusters with wS1 majorities are characterized by a transient, rapid, and sharp activation in response to the whisker stimulation (hit and miss trials), and the majority of neurons of these clusters (1, 2, and 3) are identified as sensory neurons. Clusters composed primarily of tjM1 neurons (clusters 4, 5, 7, and 8) participate in movement-related functions (hit and spontaneous licks trials) and are predominantly composed of motor related neurons. On the other hand, it is believed that mPFC plays a role in sensory input to motor output cooperating in the integration. Clusters composed primarily of mPFC neurons (clusters 6, 14, and 15) exhibit complicated behaviors that may indicate the mPFC's probable participation in learning and teaching, resulting in improved decision-making. Particularly, cluster 6 could indicate choice neurons with strong excitation in hit trials and minor activity in miss and spontaneous lick trials. Moreover, clusters 14 and 15, could show an error signal pointing to not receiving the reward.

On a different study in connectivity analysis, It has been found out that neuronal activity in wS1 and wS2 can directly affect the frontal cortex via direct monosynaptic connections with wM1 and wM2. Neuronal activity in wM1 and wM2 varied significantly during learning (Figure 28). RS units in wM1 decreased their sensory-evoked response over the course of learning, but RS units in wM2 increased their response [12]. Trial-by-trial correlations (Figure 29) and spike-triggered connectivity analyses (Figure 30) both indicated enhanced coupling between wS2-RS units and wM2-RS units, which could, at least in part, result from potentiation of monosynaptic inputs from wS2-RS units to wM2-RS units, although other more complex mechanisms could also play a role. In contrast, FS units in wM1 increased their response over the course of learning, while FS units in wM2 decreased their evoked neuronal activity. Our findings indicate that the balance between excitation and inhibition changes differentially with learning in wM1 and wM2, with improved sensory-evoked inhibition relative to excitation in wM1 and enhanced sensory-evoked excitation relative to inhibition in wM2. Changes in inhibitory neural activity may play a significant role in task learning. Throughout learning, increased recruitment of rapid inhibition in wM1 may reduce the response of excitatory neurons in wM1. It is hypothesized that inhibiting wM1 activity could improve whisker detection performance by minimizing whisker movements, which could otherwise lead to sensory reafference signals. On the other hand, the decreased firing of inhibitory neurons in wM2 during learning may permit the excitatory neurons to react more strongly.

5. Bibliography and citations

References

- [1] Emmanuel Abbe. Community detection and stochastic block models: recent developments. *The Journal of Machine Learning Research*, 18(1):6446–6531, 2017.
- [2] Rachel Aronoff, Ferenc Matyas, Celine Mateo, Carine Ciron, Bernard Schneider, and Carl CH Petersen. Long-range connectivity of mouse primary somatosensory barrel cortex. *European Journal of Neuroscience*, 31(12):2221–2233, 2010.
- [3] Michael Brecht, Miriam Schneider, Bert Sakmann, and Troy W Margrie. Whisker movements evoked by stimulation of single pyramidal cells in rat motor cortex. *Nature*, 427(6976):704–710, 2004.
- [4] Nicholas E Bush, Christopher L Schroeder, Jennifer A Hobbs, Anne ET Yang, Lucie A Huet, Sara A Solla, and Mitra JZ Hartmann. Decoupling kinematics and mechanics reveals coding properties of trigeminal ganglion neurons in the rat vibrissal system. *Elife*, 5:e13969, 2016.
- [5] Catherine S Cutts and Stephen J Eglén. Detecting pairwise correlations in spike trains: an objective comparison of methods and application to the study of retinal waves. *Journal of Neuroscience*, 34(43):14288–14303, 2014.
- [6] Victor de Lafuente and Ranulfo Romo. Neural correlate of subjective sensory experience gradually builds up across cortical areas. *Proceedings of the National Academy of Sciences*, 103(39):14266–14271, 2006.
- [7] Mathew E Diamond and Ehsan Arabzadeh. Whisker sensory system—from receptor to decision. *Progress in neurobiology*, 103:28–40, 2013.
- [8] Christian Laut Ebbesen and Michael Brecht. Motor cortex—to act or not to act? *Nature Reviews Neuroscience*, 18(11):694–705, 2017.
- [9] Ben Engelhard, Joel Finkelstein, Julia Cox, Weston Fleming, Hee Jae Jang, Sharon Ornelas, Sue Ann Koay, Stephan Y Thiberge, Nathaniel D Daw, David W Tank, et al. Specialized coding of sensory, motor and cognitive variables in vta dopamine neurons. *Nature*, 570(7762):509–513, 2019.
- [10] Vahid Esmaeili, Anastasiia Oryshchuk, Reza Asri, Keita Tamura, Georgios Foustoukos, Yanqi Liu, Romain Guiet, Sylvain Crochet, and Carl CH Petersen. Learning-related congruent and incongruent changes of excitation and inhibition in distinct cortical areas. *PLoS biology*, 20(5):e3001667, 2022.
- [11] Vahid Esmaeili, Keita Tamura, Georgios Foustoukos, Anastasiia Oryshchuk, Sylvain Crochet, and Carl CH Petersen. Cortical circuits for transforming whisker sensation into goal-directed licking. *Current Opinion in Neurobiology*, 65:38–48, 2020.
- [12] Vahid Esmaeili, Keita Tamura, Samuel P Muscinelli, Alireza Modirshanechi, Marta Boscaglia, Ashley B Lee, Anastasiia Oryshchuk, Georgios Foustoukos, Yanqi Liu, Sylvain Crochet, et al. Rapid suppression and sustained activation of distinct cortical regions for a delayed sensory-triggered motor response. *Neuron*, 109(13):2183–2201, 2021.
- [13] Arash Fassihi, Athena Akrami, Francesca Pulecchi, Vinzenz Schönfelder, and Mathew E Diamond. Transformation of perception from sensory to motor cortex. *Current Biology*, 27(11):1585–1596, 2017.
- [14] Joaquín M Fuster, Mark Bodner, and James K Kroger. Cross-modal and cross-temporal association in neurons of frontal cortex. *Nature*, 405(6784):347–351, 2000.

- [15] Lukas Grossberger, Francesco P Battaglia, and Martin Vinck. Unsupervised clustering of temporal patterns in high-dimensional neuronal ensembles using a novel dissimilarity measure. *PLoS computational biology*, 14(7):e1006283, 2018.
- [16] Matthew T Harrison and Stuart Geman. A rate and history-preserving resampling algorithm for neural spike trains. *Neural Computation*, 21(5):1244–1258, 2009.
- [17] Daniel N Hill, John C Curtis, Jeffrey D Moore, and David Kleinfeld. Primary motor cortex reports efferent control of vibrissa motion on multiple timescales. *Neuron*, 72(2):344–356, 2011.
- [18] William B Kristan Jr, Ronald L Calabrese, and W Otto Friesen. Neuronal control of leech behavior. *Progress in neurobiology*, 76(5):279–327, 2005.
- [19] Obin Kwon, Ki Woo Kim, and Min-Seon Kim. Leptin signalling pathways in hypothalamic neurons. *Cellular and Molecular Life Sciences*, 73(7):1457–1477, 2016.
- [20] Pierre Le Merre, Vahid Esmaeili, Eloïse Charrière, Katia Galan, Paul-A Salin, Carl CH Petersen, and Sylvain Crochet. Reward-based learning drives rapid sensory signals in medial prefrontal cortex and dorsal hippocampus necessary for goal-directed behavior. *Neuron*, 97(1):83–91, 2018.
- [21] Sandrine Lefort, Christian Tamm, J-C Floyd Sarria, and Carl CH Petersen. The excitatory neuronal network of the c2 barrel column in mouse primary somatosensory cortex. *Neuron*, 61(2):301–316, 2009.
- [22] Camden J MacDowell and Timothy J Buschman. Low-dimensional spatiotemporal dynamics underlie cortex-wide neural activity. *Current Biology*, 30(14):2665–2680, 2020.
- [23] Evan Z Macosko, Anindita Basu, Rahul Satija, James Nemesh, Karthik Shekhar, Melissa Goldman, Itay Tirosh, Allison R Bialas, Nolan Kamitaki, Emily M Martersteck, et al. Highly parallel genome-wide expression profiling of individual cells using nanoliter droplets. *Cell*, 161(5):1202–1214, 2015.
- [24] Valerio Mante, David Sussillo, Krishna V Shenoy, and William T Newsome. Context-dependent computation by recurrent dynamics in prefrontal cortex. *nature*, 503(7474):78–84, 2013.
- [25] Tianyi Mao, Deniz Kusefoglu, Bryan M Hooks, Daniel Huber, Leopoldo Petreanu, and Karel Svoboda. Long-range neuronal circuits underlying the interaction between sensory and motor cortex. *Neuron*, 72(1):111–123, 2011.
- [26] Johannes M Mayrhofer, Sami El-Boustani, Georgios Foustoukos, Matthieu Auffret, Keita Tamura, and Carl CH Petersen. Distinct contributions of whisker sensory cortex and tongue-jaw motor cortex in a goal-directed sensorimotor transformation. *Neuron*, 103(6):1034–1043, 2019.
- [27] Toshio Miyashita and Daniel E Feldman. Behavioral detection of passive whisker stimuli requires somatosensory cortex. *Cerebral Cortex*, 23(7):1655–1662, 2013.
- [28] Nandakumar S Narayanan and Mark Laubach. Methods for studying functional interactions among neuronal populations. In *Dynamic Brain Imaging*, pages 135–165. Springer, 2009.
- [29] Daniel H O’Connor, Simon P Peron, Daniel Huber, and Karel Svoboda. Neural activity in barrel cortex underlying vibrissa-based object localization in mice. *Neuron*, 67(6):1048–1061, 2010.
- [30] Alexis Ortiz-Rosario, Hojjat Adeli, and John A Buford. Music-expected maximization gaussian mixture methodology for clustering and detection of task-related neuronal firing rates. *Behavioural brain research*, 317:226–236, 2017.

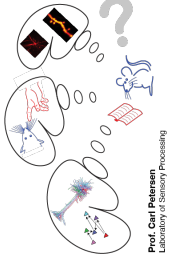
- [31] James M Otis, Vijay MK Namboodiri, Ana M Matan, Elisa S Voets, Emily P Mohorn, Oksana Kosyk, Jenna A McHenry, J Elliott Robinson, Shanna L Resendez, Mark A Rossi, et al. Prefrontal cortex output circuits guide reward seeking through divergent cue encoding. *Nature*, 543(7643):103–107, 2017.
- [32] Marius Pachitariu, Nicholas A Steinmetz, Shabnam N Kadir, Matteo Carandini, and Kenneth D Harris. Fast and accurate spike sorting of high-channel count probes with kilosort. *Advances in neural information processing systems*, 29, 2016.
- [33] Donald H Perkel, George L Gerstein, and George P Moore. Neuronal spike trains and stochastic point processes: II. simultaneous spike trains. *Biophysical journal*, 7(4):419–440, 1967.
- [34] Carl CH Petersen. The functional organization of the barrel cortex. *Neuron*, 56(2):339–355, 2007.
- [35] Lucas Pinto and Yang Dan. Cell-type-specific activity in prefrontal cortex during goal-directed behavior. *Neuron*, 87(2):437–450, 2015.
- [36] Lucas Pinto, Kanaka Rajan, Brian DePasquale, Stephan Y Thiberge, David W Tank, and Carlos D Brody. Task-dependent changes in the large-scale dynamics and necessity of cortical regions. *Neuron*, 104(4):810–824, 2019.
- [37] Ranulfo Romo and Emilio Salinas. Flutter discrimination: neural codes, perception, memory and decision making. *Nature Reviews Neuroscience*, 4(3):203–218, 2003.
- [38] Shankar Sachidhanandam, Varun Sreenivasan, Alexandros Kyriakatos, Yves Kremer, and Carl CH Petersen. Membrane potential correlates of sensory perception in mouse barrel cortex. *Nature neuroscience*, 16(11):1671–1677, 2013.
- [39] Michael N Shadlen and William T Newsome. Neural basis of a perceptual decision in the parietal cortex (area lip) of the rhesus monkey. *Journal of neurophysiology*, 86(4):1916–1936, 2001.
- [40] Markus Siegel, Timothy J Buschman, and Earl K Miller. Cortical information flow during flexible sensorimotor decisions. *Science*, 348(6241):1352–1355, 2015.
- [41] Joshua H Siegle, Xiaoxuan Jia, Séverine Durand, Sam Gale, Corbett Bennett, Nile Graddis, Gregory Heller, Tamina K Ramirez, Hannah Choi, Jennifer A Luviano, et al. Survey of spiking in the mouse visual system reveals functional hierarchy. *Nature*, 592(7852):86–92, 2021.
- [42] Tanya Sippy, Damien Lapray, Sylvain Crochet, and Carl CH Petersen. Cell-type-specific sensorimotor processing in striatal projection neurons during goal-directed behavior. *Neuron*, 88(2):298–305, 2015.
- [43] Bernt C Skottun, Russell L De Valois, David H Grosf, J Anthony Movshon, Duane G Albrecht, and AB Bonds. Classifying simple and complex cells on the basis of response modulation. *Vision research*, 31(7-8):1078–1086, 1991.
- [44] Matthew A Smith and Adam Kohn. Spatial and temporal scales of neuronal correlation in primary visual cortex. *Journal of Neuroscience*, 28(48):12591–12603, 2008.
- [45] Varun Sreenivasan, Vahid Esmaili, Taro Kiritani, Katia Galan, Sylvain Crochet, and Carl CH Petersen. Movement initiation signals in mouse whisker motor cortex. *Neuron*, 92(6):1368–1382, 2016.
- [46] Maik C Stüttgen and Cornelius Schwarz. Psychophysical and neurometric detection performance under stimulus uncertainty. *Nature neuroscience*, 11(9):1091–1099, 2008.
- [47] Naoya Takahashi, Christian Ebner, Johanna Sigl-Glöckner, Sara Moberg, Svenja Nierwetberg, and Matthew E Larkum. Active dendritic currents gate descending cortical outputs in perception. *Nature Neuroscience*, 23(10):1277–1285, 2020.

- [48] Ivan Ustyuzhaninov, Santiago A Cadena, Emmanouil Froudarakis, Paul G Fahey, Edgar Y Walker, Erick Cobos, Jacob Reimer, Fabian H Sinz, Andreas S Tolia, Matthias Bethge, et al. Rotation-invariant clustering of neuronal responses in primary visual cortex. In *International Conference on Learning Representations*, 2019.
- [49] Stella Burnham Vincent. *The Functions of the Vibrissae in the Behavior of the White Rat...*, volume 1. University of Chicago, 1912.
- [50] Moritz Von Heimendahl, Pavel M Itskov, Ehsan Arabzadeh, and Mathew E Diamond. Neuronal activity in rat barrel cortex underlying texture discrimination. *PLoS biology*, 5(11):e305, 2007.
- [51] Ulrike Von Luxburg. A tutorial on spectral clustering. *Statistics and computing*, 17(4):395–416, 2007.

A. Appendix

Experience-dependent representation of sensory-, motor- and decision-related activity in primary sensory, motor, and medial prefrontal cortical areas

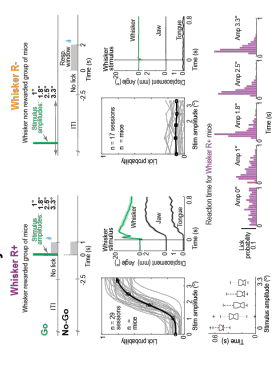
Anastasia Oryshchuk, Christos Sourmpis, Reza Asri, Vahid Esmaeili, Wulfram Gerstner, Carl C.H. Petersen and Sylvain Crochet
 Laboratory of Sensory Processing, Brain Mind Institute, EPFL, Switzerland



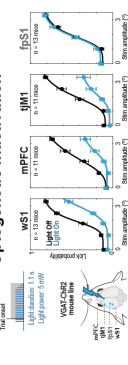
Sensory transformation during execution of goal-directed behaviors occurs through a distributed network of cortical areas. How was investigated neuronal representation of sensory, decision, and motor signals in the

whisker primary somatosensory cortex (wS1)
 - medial prefrontal cortex (mPFC)
 - tongue-jaw primary motor cortex (tJM1).
 We recorded neuronal firing extracellularly in mice trained to lick for reward in response to a brief single-whisker stimulus of varying amplitudes (Whisker R mice). To understand task-specific neuronal representations, we also recorded in another group of mice that was exposed to the same whisker stimuli, but without being associated to reward (Whisker R- mice).

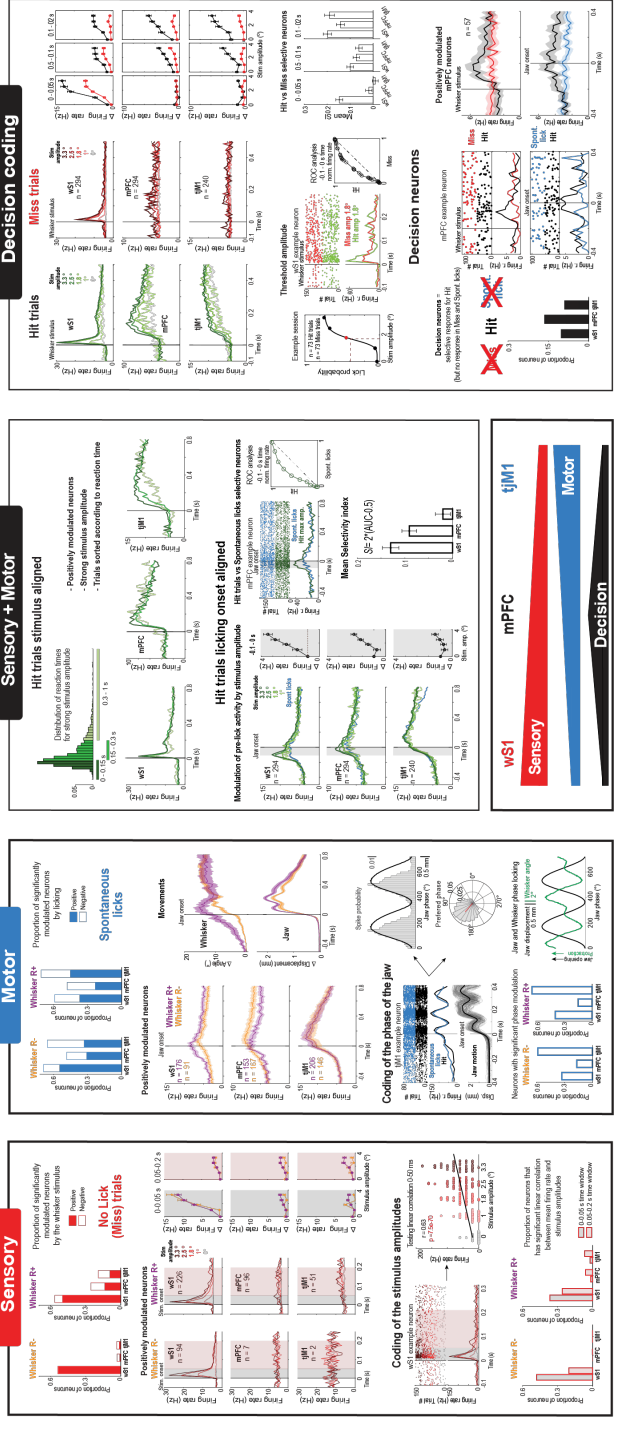
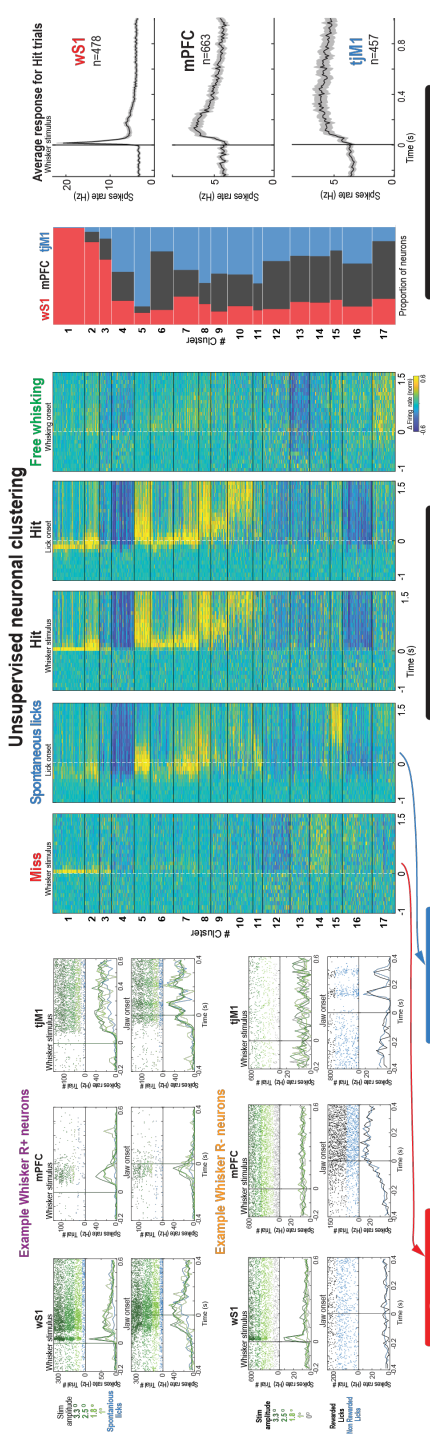
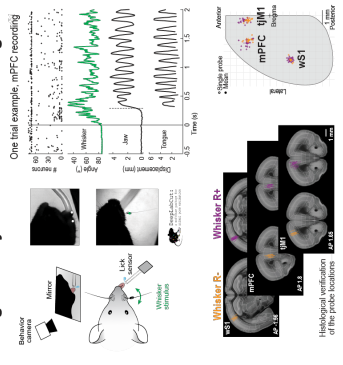
Psychometric detection task



Optogenetic inactivation








High density extracellular recordings



Goal-directed behavior requires processing of incoming sensory information, making appropriate decisions, and generating relevant motor outputs. Yet, how these diverse aspects of sensorimotor transformation arise within the intricate neuronal networks of the mammalian brain remains to be determined. Here, we investigated sensory, decision, and motor signals in the whisker primary somatosensory cortex (wS1), the medial prefrontal cortex (mPFC), and the tongue-jaw primary motor cortex (tjM1) in mice trained to lick for reward in response to a brief single-whisker stimulus of varying amplitude. Optogenetic inactivation demonstrated the causal involvement of all three areas during task execution. We then performed high-density extracellular recordings of neuronal firing in wS1, mPFC, and tjM1 of mice trained in the whisker-detection task (Trained mice). To understand task-specific neuronal representations, we recorded in another group of mice that were exposed to the same whisker stimuli, but without being associated to reward (Exposed mice). Sensory-evoked activity in the absence of licking (i.e. Miss trials) was almost exclusively found in wS1 and correlated with stimulus amplitude in both Trained and Exposed mice. All three cortical regions were strongly modulated by licking in both Trained and Exposed mice, but only tjM1 neuronal activity was unchanged comparing spontaneous (False alarms) and whisker-evoked (Hit trials) licking. Finally, decision-encoding neurons - with selective activity for Hit trials, but not Miss or False alarm trials - were found mostly in mPFC and wS1. Our results point to distinct yet inter-related roles of cortical regions for goal-directed sensorimotor transformation.

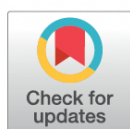
RESEARCH ARTICLE

Learning-related congruent and incongruent changes of excitation and inhibition in distinct cortical areas

Vahid Esmaeili ^{1*}, Anastasiia Oryshchuk¹, Reza Asri¹, Keita Tamura ¹, Georgios Foustoukos¹, Yanqi Liu¹, Romain Guiet ², Sylvain Crochet ¹, Carl C. H. Petersen ^{1*}

1 Laboratory of Sensory Processing, Brain Mind Institute, Faculty of Life Sciences, École Polytechnique Fédérale de Lausanne (EPFL), Lausanne, Switzerland, **2** Bioimaging and Optics Core Facility, Faculty of Life Sciences, École Polytechnique Fédérale de Lausanne (EPFL), Lausanne, Switzerland

* vahid.esmaeili@epfl.ch (VE); carl.petersen@epfl.ch (CP)



OPEN ACCESS

Citation: Esmaeili V, Oryshchuk A, Asri R, Tamura K, Foustoukos G, Liu Y, et al. (2022) Learning-related congruent and incongruent changes of excitation and inhibition in distinct cortical areas. *PLoS Biol* 20(5): e3001667. <https://doi.org/10.1371/journal.pbio.3001667>

Academic Editor: Alberto Bacci, ICM - Institut du Cerveau et de la Moelle épinière Hôpital Pitié-Salpêtrière 47, bd de l'Hôpital, FRANCE

Received: September 14, 2021

Accepted: May 10, 2022

Published: May 31, 2022

Peer Review History: PLOS recognizes the benefits of transparency in the peer review process; therefore, we enable the publication of all of the content of peer review and author responses alongside final, published articles. The editorial history of this article is available here: <https://doi.org/10.1371/journal.pbio.3001667>

Copyright: © 2022 Esmaeili et al. This is an open access article distributed under the terms of the [Creative Commons Attribution License](https://creativecommons.org/licenses/by/4.0/), which permits unrestricted use, distribution, and reproduction in any medium, provided the original author and source are credited.

Data Availability Statement: The data used to generate figures that support the findings of this study are freely available in the Open Access CERN

Abstract

Excitatory and inhibitory neurons in diverse cortical regions are likely to contribute differentially to the transformation of sensory information into goal-directed motor plans. Here, we investigate the relative changes across mouse sensorimotor cortex in the activity of putative excitatory and inhibitory neurons—categorized as regular spiking (RS) or fast spiking (FS) according to their action potential (AP) waveform—comparing before and after learning of a whisker detection task with delayed licking as perceptual report. Surprisingly, we found that the whisker-evoked activity of RS versus FS neurons changed in opposite directions after learning in primary and secondary whisker motor cortices, while it changed similarly in primary and secondary orofacial motor cortices. Our results suggest that changes in the balance of excitation and inhibition in local circuits concurrent with changes in the long-range synaptic inputs in distinct cortical regions might contribute to performance of delayed sensory-to-motor transformation.

Introduction

Many brain regions are thought to contribute to the performance of goal-directed sensory-to-motor transformations. An increasingly well-defined sensorimotor transformation studied in rodents is the learned association between a whisker sensory input and licking for reward [1–19]. From a cortical perspective considering whisker-dependent tasks requiring licking for perceptual report, sensory processing is prominent in the somatosensory cortices, whereas neuronal activity linked to motor planning during delay periods is primarily found in premotor cortices, and motor commands are more prominent in primary motor cortex [20–23]. We recently showed that in a whisker detection task with delayed licking, the correct execution of the task involves a stereotypical spatiotemporal sequence of whisker deflection-evoked neuronal firing by which sensory cortex appeared to contribute to exciting frontal cortical regions to initiate neuronal delay period activity [22]. Comparing novice and expert mice, we also found that the learning of the task is accompanied by region- and temporal-specific changes in

Figure 32: Learning-related congruent and incongruent changes of excitation and inhibition in distinct cortical areas [10]

Abstract in lingua italiana

L'interpretazione delle informazioni sensoriali in arrivo dal mondo esterno per guidare il comportamento adattivo è una funzione cruciale del cervello. Una questione fondamentale nelle neuroscienze è come e dove le informazioni sensoriali vengono tradotte in comandi motori in modo dipendente dal contesto e dall'apprendimento. Gli studi hanno dimostrato una graduale trasformazione dei segnali sensoriali in segnali decisionali/motori dalle aree sensoriali a quelle frontali: le aree sensoriali primarie codificano principalmente le caratteristiche fisiche dello stimolo, mentre la risposta delle aree frontali (come la corteccia prefrontale) covariava sia con la decisione e le caratteristiche fisiche dello stimolo. Pertanto, è stato affermato che le decisioni sensomotorie flessibili derivano dall'integrazione delle informazioni sensoriali e sul compito nella corteccia prefrontale. Si presume che la corteccia prefrontale mediale (mPFC) svolga un ruolo fondamentale nei comportamenti dipendenti dal contesto. In questo studio, è stato sviluppato un algoritmo di clustering sulla base dei dati sulla frequenza di attivazione neuronale (picchi) per raggruppare i neuroni con un comportamento simile al fine di indagare meglio la loro funzione nell'integrazione sensomotoria. È stato scoperto che esistono gruppi di neuroni wS1 e tJM1 che contribuiscono principalmente rispettivamente alla codifica sensoriale e motoria. Al contrario, altri neuroni sensoriali o motori sono diffusi in altre aree. I cluster dominati dai neuroni mPFC mostrano comportamenti complessi che possono riflettere la potenziale funzione dell'mPFC nel migliorare l'apprendimento attraverso segnali di errore (insegnamento). In uno studio separato, si studia come l'apprendimento contribuisca alla plasticità cerebrale misurando i cambiamenti nella connessione tra le regioni sensoriali e motorie durante l'apprendimento finalizzato a un compito specifico. I risultati hanno dimostrato che l'apprendimento cambia le connessioni tra i neuroni da wS1 a wM1 e da wS2 a wM1 in modo diverso.

Parole chiave: Integrazione senso-motoria, Raggruppamento neuronale, Connettività neurale

Acknowledgements

The research reported in this dissertation was undertaken between September 2021 and April 2022 at the LSENS group - Brain Mind Institute - EPFL. I'd like to thank Prof. Pedrocchi and Prof. Petersen for allowing me to embark on this journey. Thank you for having faith in me and for your support. Dear Sylvain, you have been an amazing coach. I would want to thank you for allowing me to pursue my hobbies and always ensuring that I was on the right route. This thesis would not have been possible without your contribution, incisive feedback, and supervision, Vahid, Anastasiia, and Alireza. Thank you guys!!

Lausanne, April 2022